ESL-TR-87-73
VOL II

SCALING PROBLEMS FOR WAVE PROPAGATION IN LAYERED SYSTEMS VOLUME II

F.Y. SORRELL, Y. HORIE, J.K. WHITFIELD,
S.H. LEE, J.K. PARK

NORTH CAROLINA STATE UNIVERSITY
DEPARTMENT OF MECHANICAL & AEROSPACE ENGINEERING
RALEIGH NC 27695-7910

SEPTEMBER 1989

FINAL REPORT

MARCH 1985 — MARCH 1988

AFESC

AIR FORCE ENGINEERING & SERVICES CENTER
ENGINEERING & SERVICES LABORATORY
TYNDALL AIR FORCE BASE, FLORIDA 32403

NOTICE

PLEASE DO NOT REQUEST COPIES OF THIS REPORT FROM HQ AFESC/RD (ENGINEERING AND SERVICES LABORATORY). ADDITIONAL COPIES MAY BE PURCHASED FROM:

NATIONAL TECHNICAL INFORMATION SERVICE
5285 PORT ROYAL ROAD
SPRINGFIELD, VIRGINIA 22161

FEDERAL GOVERNMENT AGENCIES AND THEIR CONTRACTORS REGISTERED WITH DEFENSE TECHNICAL INFORMATION CENTER SHOULD DIRECT REQUESTS FOR COPIES OF THIS REPORT TO:

DEFENSE TECHNICAL INFORMATION CENTER
CAMERON STATION
ALEXANDRIA, VIRGINIA 22314

SECURITY CLASSIFICATION OF THIS PAGE

REPORT DOCUMENTATION PAGE

Form Approved OMB No. 0704-0188

1a. REPORT SECURITY CLASSIFICATION UNCLASSIFIED	1b. RESTRICTIVE MARKINGS
2a. SECURITY CLASSIFICATION AUTHORITY	3. DISTRIBUTION / AVAILABILITY OF REPORT Approved for public release. Distribution unlimited.
2b. DECLASSIFICATION / DOWNGRADING SCHEDULE	
4. PERFORMING ORGANIZATION REPORT NUMBER(S) Contract F08635-85-K-0052	5. MONITORING ORGANIZATION REPORT NUMBER(S) ESL-TR-87-73 Vol II
6a. NAME OF PERFORMING ORGANIZATION North Carolina State University 6b. OFFICE SYMBOL (If applicable)	7a. NAME OF MONITORING ORGANIZATION Air Force Engineering and Services Center
6c. ADDRESS (City, State, and ZIP Code) Department of Mechanical & Aerospace Engineering Raleigh NC 27695-7910	7b. ADDRESS (City, State, and ZIP Code) HQ AFESC/RDCS Tyndall AFB FL 32403-6001
8a. NAME OF FUNDING / SPONSORING ORGANIZATION 8b. OFFICE SYMBOL (If applicable)	9. PROCUREMENT INSTRUMENT IDENTIFICATION NUMBER Contract F08635-85-K-0052
8c. ADDRESS (City, State, and ZIP Code)	10. SOURCE OF FUNDING NUMBERS PROGRAM ELEMENT NO. 6.2 / PROJECT NO. 2673 / TASK NO 0046 / WORK UNIT ACCESSION NO.
11. TITLE (Include Security Classification) Scaling Problems for Wave Propagation in Layered Systems Vol 2	
12. PERSONAL AUTHOR(S) Sorrell,F.Y.;Horie,Y.;Whitfield,J.K.;Lee,S.H.;Park,J.K.	
13a. TYPE OF REPORT Final 13b. TIME COVERED FROM Mar85 TO Mar88	14. DATE OF REPORT (Year, Month, Day) September 1989 15. PAGE COUNT 262
16. SUPPLEMENTARY NOTATION Availability of this report is specified on reverse of front cover	
17. COSATI CODES FIELD / GROUP / SUB-GROUP	18. SUBJECT TERMS (Continue on reverse if necessary and identify by block number) Keywords: Gas gun, Scaling, Layered systems, Buried model structures, Ground-shock loading, Coventional, Wave propagation, FEM

19. ABSTRACT (Continue on reverse if necessary and identify by block number)

This Technical Report consists of three volumes. Volume I, Executive Summary, Introduction and Laboratory Test Program, describes the gas gun facility and technique and correct scaling for test models. Volume II, Wave-Analysis Program for the Response of Buried Model Structures, describes the computer code for wave propagation analysis of buried model structures under ground-shock loading. Volume III, Experimental and Numerical Program, covers methods of laboratory simulation of ground shock loading from a conventional weapon and develops a unified numerical simulation of ground-shock loading and structural response.

20. DISTRIBUTION / AVAILABILITY OF ABSTRACT ☒ UNCLASSIFIED/UNLIMITED ☐ SAME AS RPT ☐ DTIC USERS	21. ABSTRACT SECURITY CLASSIFICATION UNCLASSIFIED
22a. NAME OF RESPONSIBLE INDIVIDUAL Diane B. Miller, Capt, USAF	22b. TELEPHONE (Include Area Code) (904)-283-3728 22c. OFFICE SYMBOL HQ AFESC/RDCS

DD Form 1473, JUN 86 Previous editions are obsolete. SECURITY CLASSIFICATION OF THIS PAGE

(The reverse of this page is blank.)

SUMMARY

A two-dimensional Lagrangian finite-difference computer program is developed for wave propagation analysis of buried model structures under ground-shock loading. The numerical scheme is the standard method originally proposed by von Neuman and Richtmyer, using artificial viscosity to smooth shock fronts. The program is entirely core-contained, and is limited to about 3,000 nodes because of its anticipated application on personal computers such as IBM-AT.

Material models include standard hydrodynamic-elastic-plastic relations as well as a new equation for soils and concrete.

Three model systems were considered for wave analysis: plane slabs with and without a protective soil cover and a buried model frame. The first two represent two of the idealized model tests described in Volume I. Since few dynamic data exists regarding the behaviors of the sand and microconcrete used in the construction of the model systems, the calculations were intended for generating the qualitative features of model behaviors. Nevertheless, the computational results were consistent with experimental observations and provided a rational basis for interpreting modes of failure, load profiles at concrete surface, and their interrelationships.

The wave analysis of the buried frame indicated that modes of structural failures under dynamic loading can be predicted by directly focusing on shock waves that excite the model structure.

(The reverse of this page is blank.)

PREFACE

This report was prepared by North Carolina State University, Raleigh, NC 27695-7910, under contract number F08635-85-K-0052, for the Air Force Engineering and Services Center, Engineering and Services Laboratory, Airbase Structures and Weapons Effects Branch (AFESC/RDCS), Tyndall AFB, FL 32403-6001. Lt Col Robert J. Majka and Capt Diane B. Miller were the government technical program managers. This report summarizes work accomplished between 1 March 1985 and 1 March 1988.

This report has been reviewed by the Public Affairs office and is releasable to the National Technical Information Service (NTIS). At NTIS, it will be available to the general public, including foreign nations.

This technical report has been reviewed and is approved for publication.

Diane B. Miller
DIANE B. MILLER, Capt, USAF
Project Officer

Robert J. Majka
ROBERT J. MAJKA, Lt Col, USAF
Chief, Engineering Research Division

William S. Strickland
WILLIAM S. STRICKLAND
Chief, Airbase Structures and
Weapons Effects Branch

James R. VanOrman
JAMES R. VAN ORMAN
Deputy Director, Engineering and
Services Laboratory

(The reverse of this page is blank.)

TABLE OF CONTENTS

TABLE OF CONTENTS (CONCLUDED)

LIST OF FIGURES

LIST OF FIGURES (CONCLUDED)

LIST OF TABLES

(The reverse of this page is blank.)

SECTION I

INTRODUCTION

A. OBJECTIVE

This phase of the research program, undertaken under Contract FO 8635 85K 0052, was concerned with the development of computational capabilities, primarily in support of the experimental phase of the program described in Volume I of the two-volume final report. There were two interrelated goals. The first was the development of a suitable computer program and constitutive equations to study numerically the idealized scaled model testing of buried structures through use of our gun facilities. The second was the demonstration of the applicability of the program to more realistic model structures. Special emphasis was placed on a unified treatment of topics that are traditionally analyzed separately. They are ground-shock propagation, soil-structure interactions, in-structure shock wave propagation, and failures in structural members.

B. BACKGROUND

Dynamic problems of protective structures attendant on impact and/or explosion are difficult to solve because of nonlinear differential equations involving complex geometry and materials behaviors. Therefore, traditional procedures for the design and analysis of protective structures against conventional, as well as nuclear weapons, have been separated into two or three distinct stages (References 1 and 2). For instance, in the case of blast or ground-shock loading, the procedure involves two separate steps. The first is the determination of equivalent loads from blast or ground shock at a prescribed standoff distance. The second is the design analysis and performance predictions of a given structure, based upon the equivalent loads, by assuming an equivalent single- or multidegree of freedom system.

Recent improvements in the development of predictive and analysis techniques have been mostly numerical and involve computer simulation of the dynamic problems by use of finite element and finite difference methods (References 3-6). Large-scale computations have come into widespread use in structural and ordnance designs. These methods have now been developed to a point where they can handle complex shapes, large deformations, and failures involved in problems of impact and explosion. The principal limitation in the use of these numerical methods is said to be largely the uncertainty in the description of meterials behavior (Reference 3). If the response model is inadequate, they are known to provide solutions which are not even qualitatively correct. Therefore, effective use of any of the numerical techniques requires iterative adjustments of material models in close collaboration with material and structural testings.

The present investigation leading to this report is an initial attempt of similar type to analyze and aid in the design of the scaled model testing of buried concrete structures by use of a finite difference computer program.

C. SCOPE/APPROACH

Many computer codes are available for the analysis of transient problems associated with impact and explosions (References 4-11). Our computer program is a two-dimensional explicit finite difference code in plane geometry and is derived from other codes of this type which are known by their acronyms as HEMP, TWOODY, STEALTH, and TROTT. Special features of the code are :

- the code is core-contained,
- the cell layout is easy,
- the code can be easily modified for new materials models.

However, it is restricted in the size of problems that can be treated and does not contain features such as slide lines, rezoning, and buffering of cell variables that are common in large general-purpose codes described above.

Constitutive models in the program are presently limited to: (1) a standard hydrodynamic-elastic-plastic model for solids and (2) a model specially developed for soils and concrete. The latter is developed to deal with the influence of porosity on the inelastic behavior of materials in a physically consistent manner so that phenomena such as shear enhanced pore compaction can be represented. New models will be added as needs arise. For instance, a high-explosive equation of state will be included in the near future to consider the scaled model simulation of buried structures under close-in detonations.

Two model systems were investigated numerically: plane slabs with and without a protective soil cover and a buried model frame. The explosive loading on these structures was simulated by a shock-wave loading described in Volume I of the final report. Selected results from the numerical simulation of the plane slabs were compared with data obtained in the experimental phase of the project. They are a qualitative description of failure modes, ground-shock propagation in the soil cover, and structural response behaviors of the model structures. However, because of limited experimental data, no systematic attempt was made to fit the experimental data numerically by optimizing material parameters in constitutive equations. The principal goal of the calculations was to demonstrate the capabilities of the code.

The remainder of this report is divided into three sections. Section II presents a summary of basic continuum mechanics equations for describing two-dimensional stress wave propagation through solid and porous materials such as soil. This section also describes the algorithms used to solve the basic equations by using an explicit finite difference method. Section III describes the numerical investigation of ground-shock propagation in simple layered systems: plane slabs with and without protective soil cover and a

buried frame. Selected results from the first example were compared with experimental results reported in Volume I of the final report. Section IV presents the conclusions reached from the sample simulations.

SECTION II

CODE DESCRIPTION

A. BASIC EQUATIONS

The mathematical description of transient dynamical problems attendant on impact and detonations consists of the conservation laws of physics, initial and boundary conditions, and material models. The finite difference technique is an approximate method of solving these equations using discretized time and space coordinates. The Lagrangian method is based upon a coordinate system that moves with the material. It has been developed to a point where general-purpose codes are now capable of handling large-scale simulations involving 50,000 nodes. Since there are many excellent expositions of the Lagrangian technique for stress wave propagation in one-, two-, and even three dimensions (References 7-11), what follows is a summary description of the basic equations and computational procedures involved in our code. For details, readers are referred to the References described above. But, an exception will be made in the description of the material model for soils and concrete because of its importance in the solution of problems of interest.

1. Conservation Equations

a. Conservation of Mass

The equation expressing the conservation of mass is

$$u_{,x} + v_{,y} = \dot{A}/A \tag{1}$$

where u and v are the components of velocity in rectilinear Lagrangian coordinates (x,y), $\dot{A}/A$ is the aerial strain rate, the dot "." signifies the partial time derivative, $u_{,x} = \partial u/\partial x$ and $u_{,y} = \partial v/\partial y$. The volumetric strain rate is related to the density change as follows:

$$-(\partial\rho/\partial t)/\rho = u_{,x} + v_{,y} + W_{,z}$$

$$= \dot{A}/A \text{ in plane } x - y \text{ geometry} \qquad (2)$$

where $1/\rho = V$ = the specific volume, and W is the velocity component in the z-axis (zero in plane geometry).

The local strain rate is defined as the symmetric part of the velocity gradient.

$$\dot{\varepsilon}_{xx} = u_{,x}$$

$$\dot{\varepsilon}_{yy} = v_{,y}$$

$$\dot{\varepsilon}_{xy} = (v_{,x} + u_{,y})/2.$$

The local rotation rate is defined by

$$\dot{\omega}_{xy} = (v_{,x} - u_{,y})/2.$$

b. Conservation of Momentum

The equations expressing the conservation of momentum are

$$\rho\dot{u} = \sigma_{xx,x} + \sigma_{xy,y} - q_{,x} \qquad (3)$$

$$\rho\dot{v} = \sigma_{xy,y} + \sigma_{yy,y} - q_{,y} \qquad (4)$$

where ρ is the density, $\dot{u}$ and $\dot{v}$ are the components of acceleration, σ_{xx}, σ_{xy}, and σ_{yy} are the stress components, and q the artificial viscosity. The sign convention for the stress components is positive for tension. Pressures are positive for compression.

Inclusion of the artificial viscosity term in the momentum equations is now a standard technique of han ıg discontinuous shock 'waves numerically, by rendering the solution continuous using viscous effects. However, care is necessary so that the viscous term does not affect the solution anywhere except at shock fronts. In our code the main artificial viscosity term consists of linear and quadratic bulk viscosity components given by

$$q = \begin{cases} b_1 C_s A^{1/2} \rho_{,t} + b_2^2 A(\rho_{,t})^2/\rho & \text{for } r_{,t} > 0 \\ 0 & \text{for } p_{,t} \leq 0 \end{cases} \tag{5}$$

where b_1 and b_2 are constants and C_s is the speed of sound given by

$$C_s = (\partial r/\partial \rho)_s^{1/2} \tag{6}$$

where s indicates the differentiation at constant entropy.

When a large distortion of computational cells is encountered, additional viscosities are included in the deviatoric stress components. They are devised to minimize hour-glass shaped distortion of quadrilateral cell elements. This distortion is a consequence of the fact that the quadrilateral cell used in plane geometry has eight degrees of freedom, but that only six are accounted for in the basic equations that provide resistance to these motions. In some codes these viscosities are known as the triangular artificial viscosity. These triangular stresses are

$$q_{xx} = b_3 A^{1/2} C_s \rho (2 \dot{\epsilon}_{xx} - \dot{\epsilon}_{yy}) \tag{7}$$

$$q_{yy} = b_3 A^{1/2} C_s \rho (2 \dot{\epsilon}_{yy} - \dot{\epsilon}_{xx}) \tag{8}$$

$$q_{xy} = 3 b_3 A^{1/2} C_s \rho \dot{\epsilon}_{xy} \tag{9}$$

where b_3 is a constant. These stresses are added to the stresses obtained from the constitutive equations described in the next section.

c. Conservation of Energy

The following expression of the conservation of energy ignores thermal heat conduction. This is a reasonable approximation for the time scale involved in stress wave propagation.

$$\dot{E} = - (p + q) \dot{V} + V(s_{xx} \dot{\varepsilon}_{xx} + s_{yy} \dot{\varepsilon}_{xy} + s_{zz} \dot{\varepsilon}_{zz} + 2 s_{xy} \dot{\varepsilon}_{xy}) \quad (10)$$

where E is the specific internal energy, p the pressure, s_{xx}, s_{xy}, and s_{yy} are the deviatoric stress components defined by

$$s_{ij} = \sigma_{ij} + p \quad (11)$$

where i and j stand for x and y.

2. Constitutive Equations

The present program contains two material models. They are a standard hydrodynamic-elastic-plastic model for solids and a special model for porous media such as soil and concrete. The former model was initially developed for the description of metallic materials, but it has been effectively used even for materials such as concrete in a certain range of impact conditions (Reference 13).

In stress wave calculations, it may be necessary to permit fracture of materials (say, spalling) during the calculations. An effective representation of such a separation may be provided by letting the stress in the cells along one side to reduce to zero. The algorithm is described in Section IIB.

a. Hydrodynamic-elastic-plastic model

In this standard model the stress tensor σ_{ij} is resolved into the pressure and deviatoric stress tensors as follows (same as Equation (11).

$$\sigma_{ij} = s_{ij} - p.$$

The hydrostatic pressure p is described by a Mie-Gruneisen equation given by

$$p = f_1(\rho) + \rho \Gamma E \tag{12}$$

where Γ is the Grüneisen ratio and $f_1(\rho)$ is written in terms of a polynomial function:

$$f_1(\rho) = a_1(\eta - 1) + a_2(\eta - 1)^2 + a_3(\eta - 1)^3 \quad , \tag{13}$$

where $\eta = \rho/\rho_o$, and ρ_o = initial density.

The deviatoric stress components account for elastic behaviors and are calculated by the frame-indifferent isotropic elasticity equations (Reference 12),

$$\overset{\nabla}{S}_{ij} = 2 \mu \dot{e}^{e}_{ij} \tag{14}$$

$$\overset{\nabla}{S}_{ij} = \dot{s}_{ij} - \omega_{ik} s_{kj} + \omega_{kj} s_{jk} \tag{15}$$

where $\overset{\nabla}{S}_{ij}$ is the co-rotational stress rate, μ, shear modulus, ω_{ik} is the component of the rotation tensor, and e^{e}_{ij} are the elastic deviatoric strain components defined by

$$e_{ij} = \varepsilon_{ij} - (1/3) \varepsilon_{kk} \delta_{ij} \, . \tag{16}$$

n plane geometry Equations (14) and (15) reduce to

$$\dot{s}_{xx} = 2\mu\, e_{xx} + 2\,\omega\, s_{xy}$$
$$\dot{s}_{yy} = 2\mu\, e_{yy} + 2\omega\, s_{xy}$$
$$\dot{s}_{xy} = 2\mu\varepsilon_{xy} - \omega(s_{xx} - s_{yy}) \qquad (17)$$

here $\omega = \omega_{xy}$ = local rotation about the z-axis.

The transition from an elastic to a plastic state is letermined by the Von Mises yield function

$$g(\sigma_{ij}) = s_{ij}s_{ij} - 2Y^2/3 \ . \qquad (18)$$

here Y is the yield stress in simple tension. The material is elastic if $g < 0$, and plastic if $g = 0$, whereas the condition $g > 0$ can never be ealized. In the plastic state it is assumed that the total strain rate is he sum of the elastic and plastic strain rates and that the plastic strain ate is determined by an associated flow rule such that

$$\dot{\varepsilon}_{ij} = \dot{\varepsilon}^{e}_{ij} + \dot{\varepsilon}^{p}_{ij} \qquad (19)$$

$$\dot{\varepsilon}^{p}_{ij} = \dot{\lambda}(\partial g/\partial\sigma_{ij}) \qquad (20)$$

In this formulation the plastic strain rate becomes normal to the yield surface as expressed by Equation (18). This relationship provides an expedient algorism for evaluating stress increments in plastic state.

b. Model for Porous Materials

Continuum plasticity has long been used for modeling the mechanical behaviors of geological materials such as soils and rocks (References 14 and 15). Recent models involve a complex combination of mutiplastic potential surfaces and a nonassociated flow rule (References 16-

18). However, as the complexity of these model increases, so does the difficulty of determining their material parameters. It is not uncommon to find a model with more than two dozen adjustable parameters. With this many parameters, their determination is rarely complete, particularly when various paths are involved in loading, as well as in unloading.

The model in our code was originally proposed by Swegle (Reference 19) as an extension of the hydrodynamic P-α model to include shear strength in the description of porous materials including geological materials. The most important feature of this model is its simplicity. Our investigations (References 20-21) showed that as few as two to four free parameters are sufficient to deal with materials such as metal and ceramic powders as well as various types of soil. Other noteworthy features are: (1) the description of overall stress in terms of the stress in solid components and porosity, and (2) the use of associated hardening flow rule to describe coupling between volumetric and deviatoric inelastic behavior.

The following is a summary of Swegle's formalism in incremental form.

a. Stress

Effective stress components are determined by those of the solid components and the solid volume fraction α as follows:

$$\sigma_{ij} = -p\delta_{ij} + s_{ij} \tag{21}$$

$$p = \alpha p_s = \alpha f(V_s, E) \tag{22}$$

$$s_{ij} = \alpha s_{ijs} \tag{23}$$

where $\alpha = V_s/V$, the subscript "s" stands for the solid.

b. Strain

Strain components are partitioned in terms of volume components, i.e.,

$$d\varepsilon_{ijs} = (d\theta_s/d\theta)d\varepsilon_{ij} \tag{24}$$

where

$$d\theta = dV/V \text{ and } d\theta_s = dV_s/V_s \ . \tag{25}$$

It can be shown that, if the above partition of the strain components is used, then irrespective of deformation modes,

$$de_{ijs} = de_{ij}[1 + (d\alpha/\alpha)(dV/V)^{-1}] \ . \tag{26}$$

where

$$de_{ij} = \alpha\varepsilon_{ij} - (d\theta/3)\ \delta_{ij} \ . \tag{27}$$

c. Elastic regime

Elastic response is formulated by use of the P-α model and a frame indiffernet isotropic Hooke's law. That is,

$$(d\alpha/dP)_{elastic} = [1/h^2(\alpha) - 1]/K_o \ , \tag{28}$$

where

$$h(\alpha) = 1 + [(1 - \alpha).(1 - \alpha_o)](C_o/C_{so} - 1) \tag{29}$$

K_{so} = solid bulk modulus at zero pressure,
C_o, C_{so} = sound velocities at zero pressure,

$$ds_{ijs} = 2G_s de_{ijs} + (\omega_{ik}s_{kj} - \omega_{kj}s_{ik})dt, \tag{30}$$

d. Plastic Regime

Plastic state of the material is determined by a yield function similar to that of the perfectly plastic solid described in the previous section. That is,

$$g = f(J_1, \sqrt{J_2'}, \alpha) \tag{31}$$

where

$$J_1 = \sigma_{KK} = -3p \ , \tag{32}$$

and

$$\sqrt{J_2'} = (1/2\ s_{ij}s_{ij})^{1/2} \ . \tag{33}$$

The material behaves elastically if

$$g \leq 0 \tag{34}$$

and plastically if

$$g = 0 \ . \tag{35}$$

Then, the plastic strain increment is prescribed by the associated flow rule such that

$$d\varepsilon_{ij} = d\varepsilon_{ij}^{e} + d\varepsilon_{ij}^{p} \tag{36}$$

$$d\varepsilon_{ij}^{p} = d\lambda\ (\partial g/\partial \sigma_{ij}) \tag{37}$$

where the superscript describes the state of the material.

There are many potential yield functions including the well known Mohr-Coulomb and Drucker-Prager models for the description of porous materials. Based upon our experience (References 20-21), the present code contains only the elliptic yield function described below. But, we also tested a lemniscate function for future study. Results with the latter function are given in Appendix A.

e. Elliptical Yield Function

$$g = \left[\left(p - p_m(\alpha)\right) / \rho_1(\alpha)\right]^2 + \left[\left(3 J_2'\right)^{1/2} / Y_1(\alpha)\right]^2 - 1 \qquad (38)$$

where

$$p_m(\alpha) = (p_1(\alpha) - K(\alpha)) / 2$$
$$p_1(\alpha) = (p_p(\alpha) + K(\alpha)) / 2$$
$$K(\alpha) = K_o + c p_p(\alpha)$$
$$Y_1(\alpha) = Q_o(1 - \alpha)^m p_p(\alpha)$$
$$p_p(\alpha) = (y/\beta)\left[(1 - \alpha)^{-2\beta/3} - c_p\,(1 - \alpha_o)^{-2\beta/3}\right]$$

and c, Q_o, m, Y, β, and c_p are constants.

These selections have been made based upon the observations (References 20 and 21) that they describe the general features of yield surfaces which are observed experimentally and that their parameters can be understood through mechanistic interpretation of flow mechanisms. For example the current form of $\rho_p(\alpha)$, which is the hydrostatic inelastic compression of porous material, is determined based upon a spherical pore-collapse model. Detailed descriptions of this model are found in Reference 20.

3. Boundary and Initial Conditions

Boundary conditions in a layered system may be divided into two distinct categories: external and internal boundaries. Typically, external

conditions are specified in terms of stress or velocity components for all boundary points. Common examples are a free surface or a smooth rigid wall (zero velocity in the direction normal to the wall surface). Normally, boundary conditions at an internal interface are the standard continuity conditions for normal stress and velocity. But, they could become very complex if interfacial motions such as sliding, opening, and closing are included. In the current code, only the separation of an interface in one spatial direction is treated. It is an approximate representation through use of the crack opening described in Section IIB.

Initial conditions must be given for all dependent variables to determine the subsequent motions. That is, the initial state of stress and strain, as well as geometry, must be known.

B. COMPUTATIONAL PROCEDURES

In a finite difference approach one starts with the governing differential equations and approximates them by appropriate discrete equations based on computational grid or mesh. Our Lagrangian explicit scheme is derived basically from that found in several general-purpose large codes (References 8-12). Therefore, no attempt will be made to duplicate excellent discussions found in these references. We will limit our remarks to a description of the inner working of our code.

1. Integration of Governing Equations

Figure 1 illustrates our finite-difference grid arranged in a staggered rectangular array indexed by i and j. Kinematic quantities dealing with motion such as positions are defined at integer locations. The remaining quantities such as stress, strain, and internal energy are calculated at half-integer points as averages over a cell volume or a surface area. For example, $x_{j,i}$ represents a Lagrangian position at time, say $t = t^n$ and $\sigma_{j+1/2,\ i+1/2}$ a stress component for the quadrilateral cell having corners at (j,i), (j+1), i), (j+1, i+1), and (j, i+1).

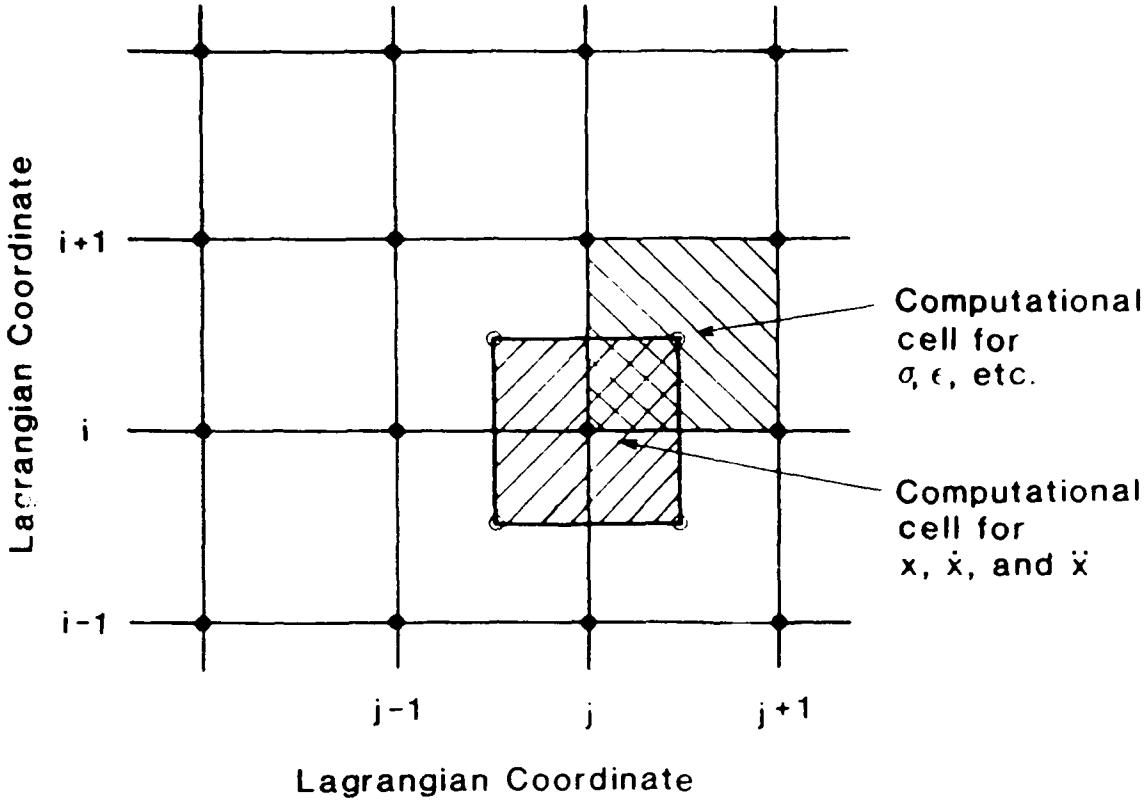

Figure 1. Computational Grid Showing Locations of Cells for Computing Kinematic and Equation-of-State Variables

The integration of the dynamic equations is based upon the standard leap-frog method and proceeds as follows. Initially or at time $t = t^n$, all quantities are defined at all points by the initial conditions or previous calculations. Computations to advance one time step from t^n to t^{n+1} is done in four steps, as illustrated in Figure 2. First, the momentum equation, Equations 3 and 4 are solved for the new acceleration at $t = t^n$. If $\ddot{x}_{j,i}$ were the acceleration being calculated, the quantities required are specified at neighboring four half-integer points. These points comprise a computational cell for motion variables as illustrated in Figure 1. Then, the resulting acceleration is used to calculate the new velocity and position, $\dot{x}^{n+1/2}_{j,i}$ $x^{n+1}_{j,i}$ by using time-centered integrations.

COMPUTATIONAL SEQUENCE

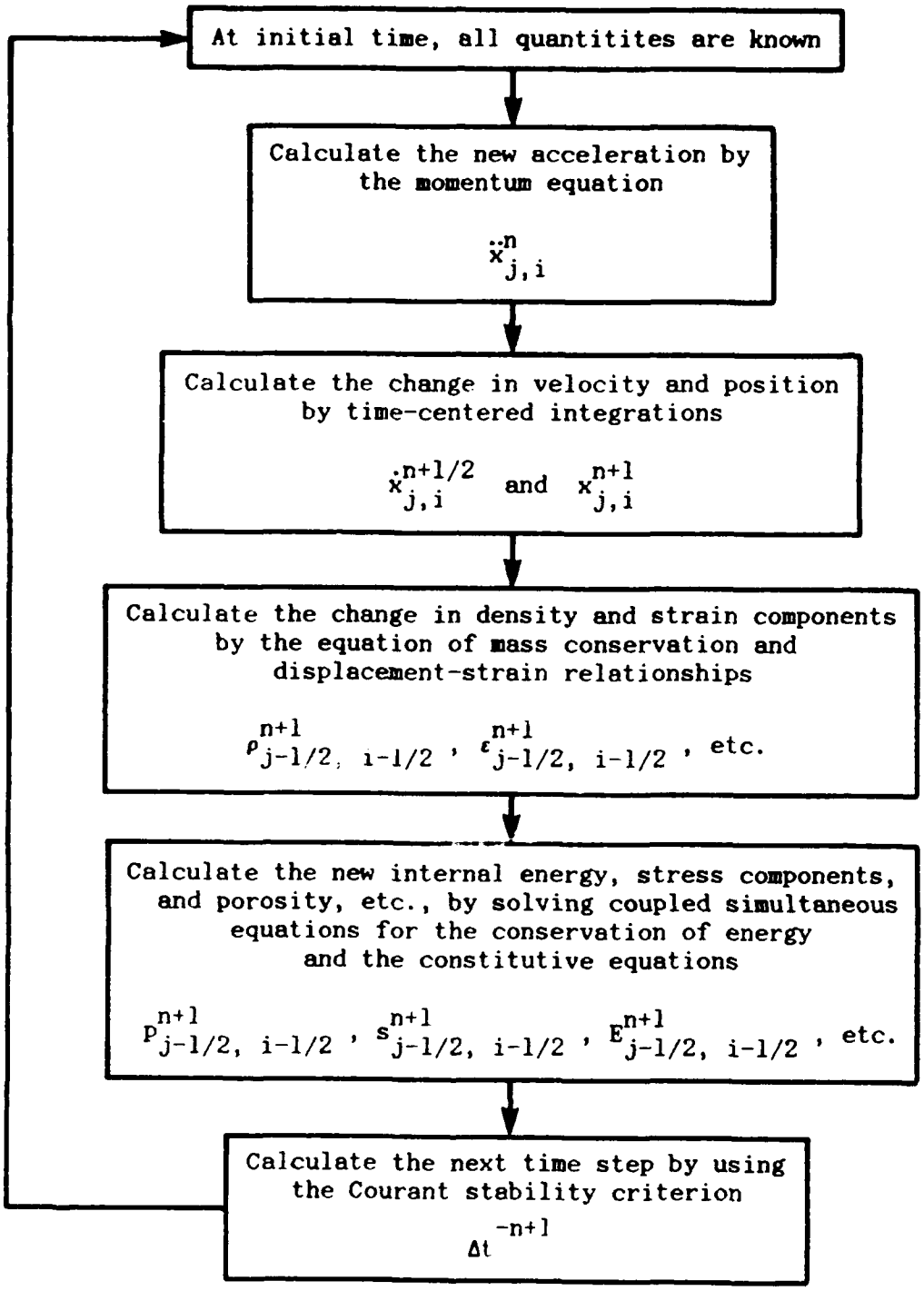

Figure 2. Computational Sequence for One Time-Cycle

$$\dot{x}^{n+1/2}_{j,i} = \dot{x}^{n-1/2}_{j,i} + \ddot{x}^{n}_{j,i}\,\Delta t^{n} \tag{39}$$

$$x^{n+1}_{j,i} = x^{n}_{j,i} + \dot{x}^{n+1/2}_{j,i}\,\Delta t^{n+1/2} \tag{40}$$

where $\Delta t^{n} = t^{n+1}$ and $\Delta t^{n+1/2} = t^{n+1/2} - t^{n}$.

The order in which computations are performed is such that at the time the position of $x^{n+1}_{j,i}$ is computed, the positions and velocities at the other vertices of the quadrilateral cell having smaller j and i are already known. A schematic of the order is shown in Figure 3.

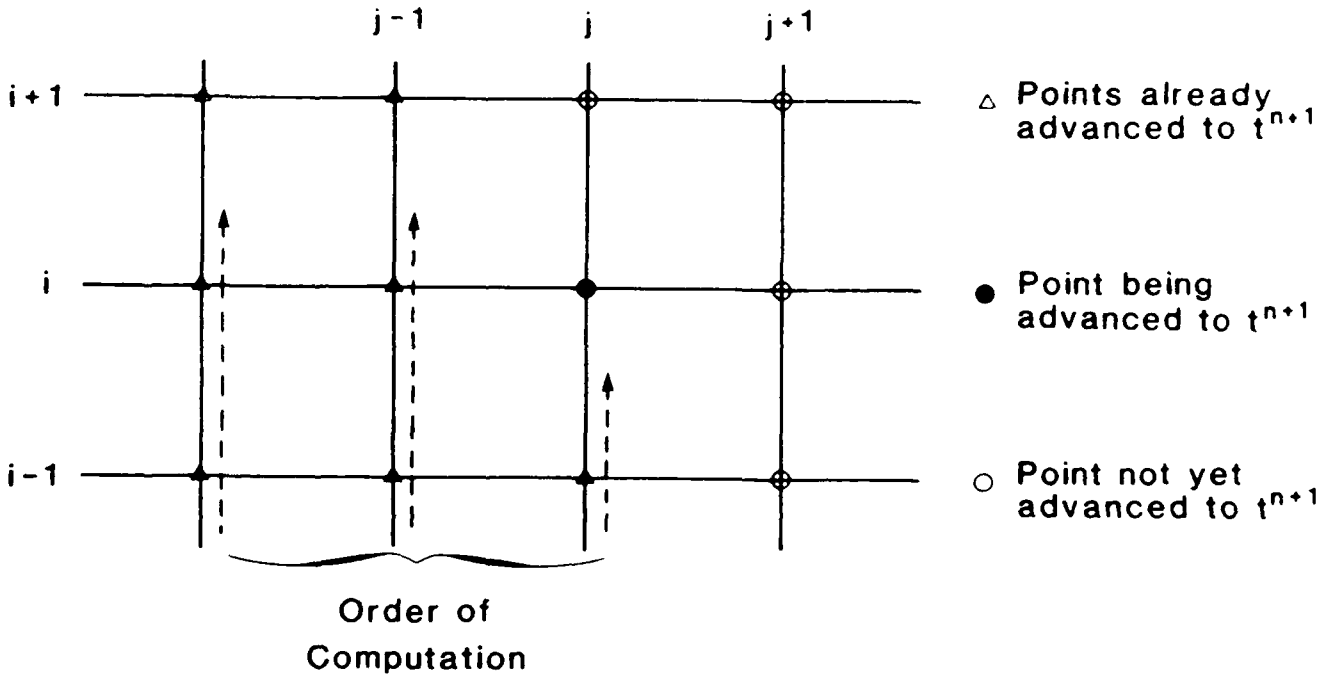

Figure 3. Schematic Representation of the Order of Computation

In the second step, we use those new positions at $t = t^{n+1}$ to calculate the new density and strain components from the equation of mass conservation and displacement-strain relationships, respectively. These quantities are calculated as averages over a computational cell shown in Figure 1.

In the third step, using the new density and strain components, the energy equation and constitutive equations are simultaneously solved for the new stress components, internal energy, and other constitutive variables such as porosity. Depending upon the complexity of the constitutive equations, these simultaneous equations may involve a system of nonlinear coupled ordinary differential equations and require a lengthy iterative scheme to find solution.

The fourth step is a preparation for the next time cycle and evaluates the next time increment based upon the Courant stability condition,

$$\Delta t = t^{n+1} - t^{n} \leq \Delta x / C_s \tag{41}$$

where Δx = the minimum cell dimension.

In our program, this equation is modified to include the effect of the artificial viscosity as follows (Reference 12).

$$\Delta t = \min (\Delta x / C_e)(1 - 3b_3) \tag{42}$$

where C_e is the local sound speed.

2. Boundary Conditions

The procedure described in the previous section applies to a point in the interior of the homogeneous Lagrangian grid. At exterior or interior boundaries the algorisms must be modified. Currently, only a limited number of boundary conditions is provided in our program. Two kinds of exterior boundary conditions are considered. These are a rigid but smooth wall and a free surface. A rigid wall (or boundary) is represented by setting the velocity of mesh points in a prescribed direction to zero. But no constraint is imposed on the motion of the mesh points in the direction parallel to the wall. At a stress free boundary, since the stress components are calculated

as averages over a computational cell, a massless "phantom" zone is created beyond the "real" zone. The coordinates of the outside vertices of the phantom cell are arbitrary and are normally set equal to the coordinates of the points on the real surface.

For interior boundaries the present version of the code cannot treat sliding internal interfaces. Therefore, mesh points at an internal boundary are considered to be common to both sides of the interface and have the averaged mass of the adjacent materials. However, an effective representation is provided for a separating interface in one direction by letting the stress in the cell along one side reduce to zero. This procedure can also be used to represent approximately the creation of a crack in the interior of the material. The behavior of cracked material is simulated by adjusting the stress in the cell so that there is no normal stress across the crack. But, since a Lagrangian cell having cracks is not allowed to separate into several pieces, the stress in it is adjusted to the value appropriate to such cracked material. This is achieved by the following stress adjustments.

$$\sigma_{xx} \rightarrow 0$$

$$\sigma_{yy} \rightarrow \sigma_{yy} + \lambda \Delta\varepsilon$$

$$\sigma_{zz} \rightarrow \sigma_{zz} + \lambda \Delta\varepsilon$$

$$\sigma_{xy} \rightarrow 0 \qquad (43)$$

where λ is a Lame's constant and $\Delta\varepsilon = -\sigma_{xx}/(\lambda + 2\mu)$.

C. INPUT AND OUTPUT

Since our computer program is a special purpose code, input and output data are kept to a minimum amount necessary for solving two-dimensional stress wave propagation through layered systems. The input data consist of

general running and printing instructions, materials data, grid layout data, and initial conditions. The instructions for the input data preparation are described in Appendix B.

Because of our emphasis on load profiles, the current output are limited to stress components, positions, and particle velocities. However, the program can be easily modified to print other variables including time histories of dependent variables.

SECTION III

SAMPLE CALCULATIONS

Two types of problems were considered for sample calculations to test the computer program. The first is the calculation of stress wave propagation in two of the model tests described in Volume I of the final report. The second is the analysis of the model testing of a more realistic, but hypothetical buried structure. However, since few dynamic data exist regarding the behavior of the model sand and microconcrete, the calculations were intended only for generating the qualitative features of model behaviors.

A. SCALED MODEL SLABS

Two experiments were selected for sample calculations. They are M014 and M022. The major goals of these shots were: (1) to demonstrate the capabilities of producing a selected failure mode, say, spalling, by tailoring shock pulses and (2) to study the influence of a protective layer on failure modes as well as on shock profiles (magnitude, time history, etc). In these experiments, the dynamic loading was modeled by impact of a projectile fired from a gas gun and tailored by the projectile size, speed, material, mass, etc. An idealized test configuration used for the simulation is shown in Figure 4.

Materials properties used for simulation of these tests are summarized in Table 1. However, since no systematic experiments were conducted for the purpose of generating dynamic material data in this phase of the research program, no attempt was made to optimize these properties to fit experimental results. Elastic properties are those found in standard handbooks. Inelastic properties of Lexan®, aluminum, and microconcrete were determined using the von Mise criterion and stress for tensile failure (Reference 22). The use of the perfectly plastic model for the concrete was solely due to the lack of dynamic data. When data becomes available, it will be replaced by the porous model. The material constants for the sand

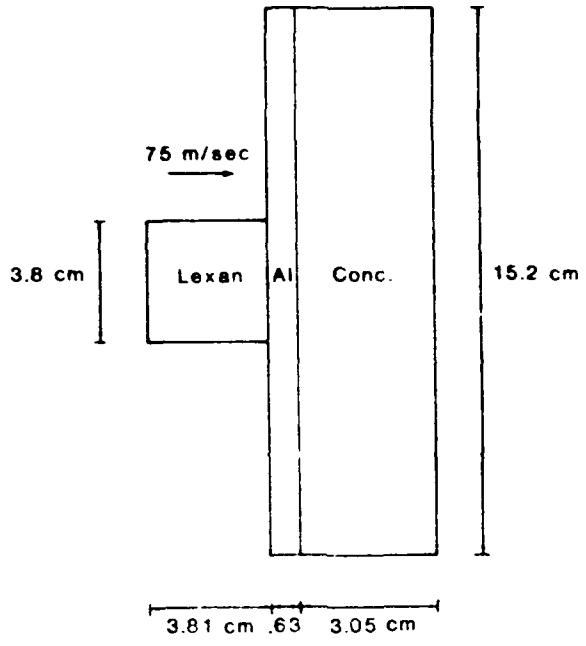

(a)

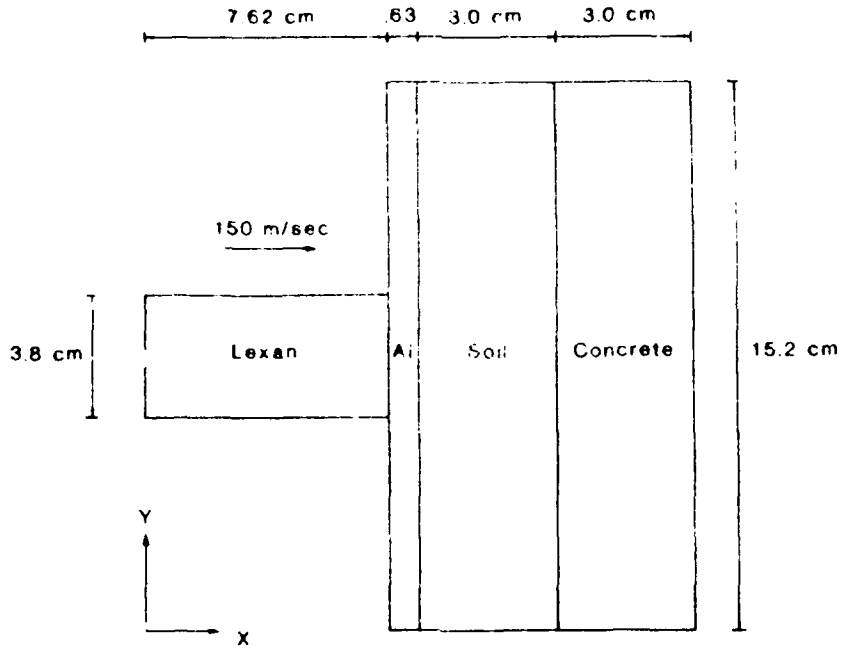

(b)

Figure 4. Test Configurations Idealized for Numerical Calculations

TABLE 1. MATERIAL PROPERTIES OF ALUMINIUM, LEXAN AND CONCRETE

	Aluminium	Lexan	Concrete*
Bulk Modulus (Gpa)	80	3.47	13.1
Shear Modulus (Gpa)	30	0.90	9.4
Density (kg/m^3)	2780	1190	1080
Sound Speed (m/sec)	6560	1980	3510
Yield Strength (Mpa)	75	7	28

*Cunningham, C. H., Townsend, F. C., and Fagundo, F. E., "The Development of Micro-Concrete for Buried Structrures," University of Florida, Gainesville, 1986.

were generated through use of Hugoniot data (Reference 23) and our data on wave arrival times in the pressure range of 1-5 kb. Figure 5 compares of the Hugoniot data with those generated by computer simulation of shock wave propagation in the model sand. For the particle velocity of less than 0.2 mm/ μsec, waves were too dispersed to define a meaningful shock front. The calculated Hugoniot at 2 kb was fitted to that estimated from the wave arrival times.

1. Shot M0 14

Figures 6-10 illustrate selected results from the simulation of Shot M0 14 where a concrete slab was shock loaded without a protective sand layer (see Figure 4(a)). The aluminum layer was used to prevent impact damages on the concrete surface. The length of the projectile was arbitrarily reduced to one half of the original length to save computer time. This change has no influence on the early-time solutions shown in Figures 6-10. In this simulation the separation of the interface between aluminum and concrete was provided by using the procedure discussed in Section IIB. Also, the edges of the plates were assumed to be free.

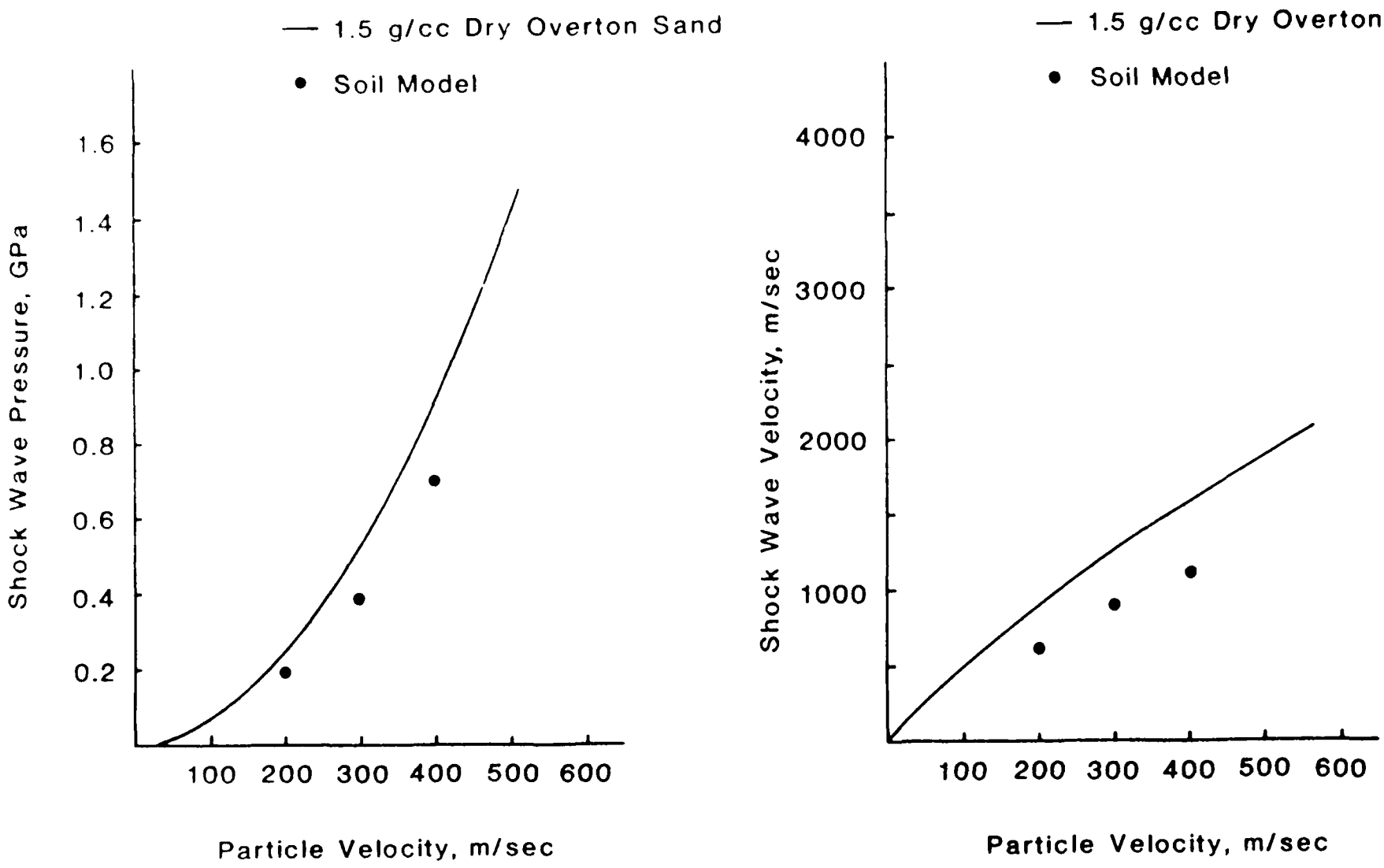

Figure 5. Comparison of the Calculated Hugoniot Data of The Model Sand with Those of Dry Overton Sand (Reference 23). Calculated Shock-Wave Velocities Were Fitted to Match Those Measured in the Model Sand.

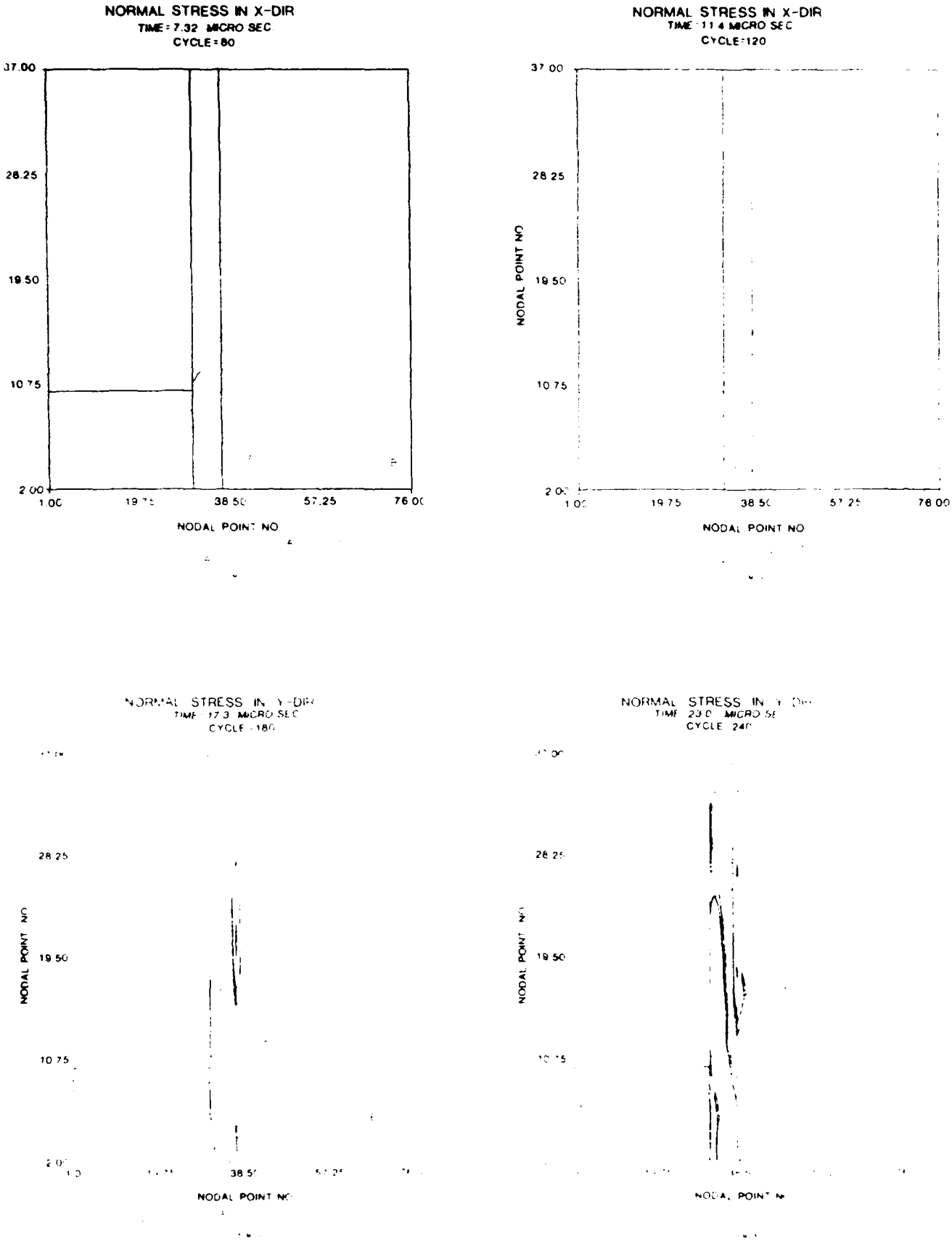

Figure 6. Temporal Evolution of Normal Stress (σ_{xx}) in the Longitudinal Cross Section. Impact Velocity = 75 m/sec

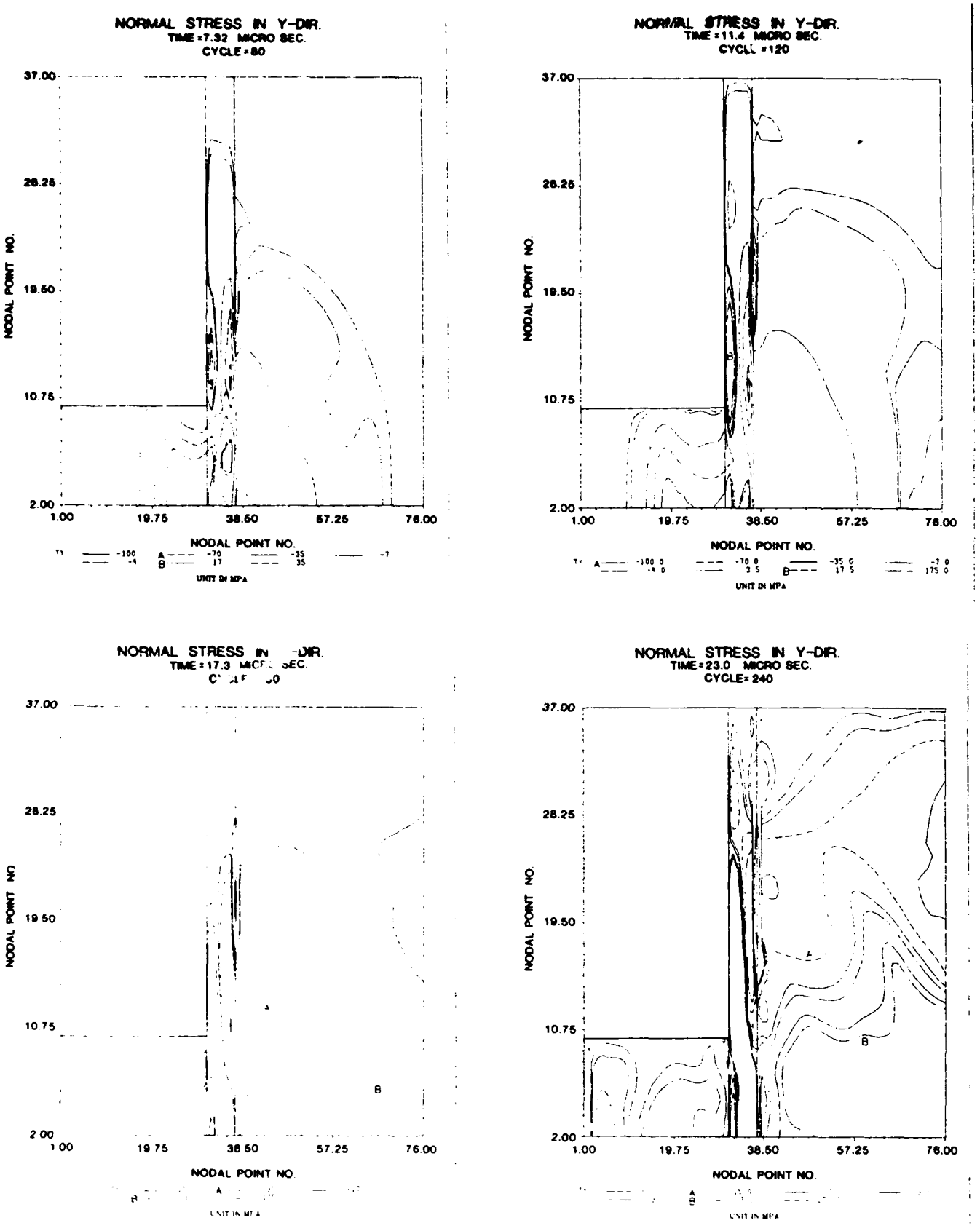

Figure 7. Temporal Evolution of Normal Stress Distribution (σ_{xx}) in the Longitudinal Cross Section. Impact Velocity = 75 m/sec

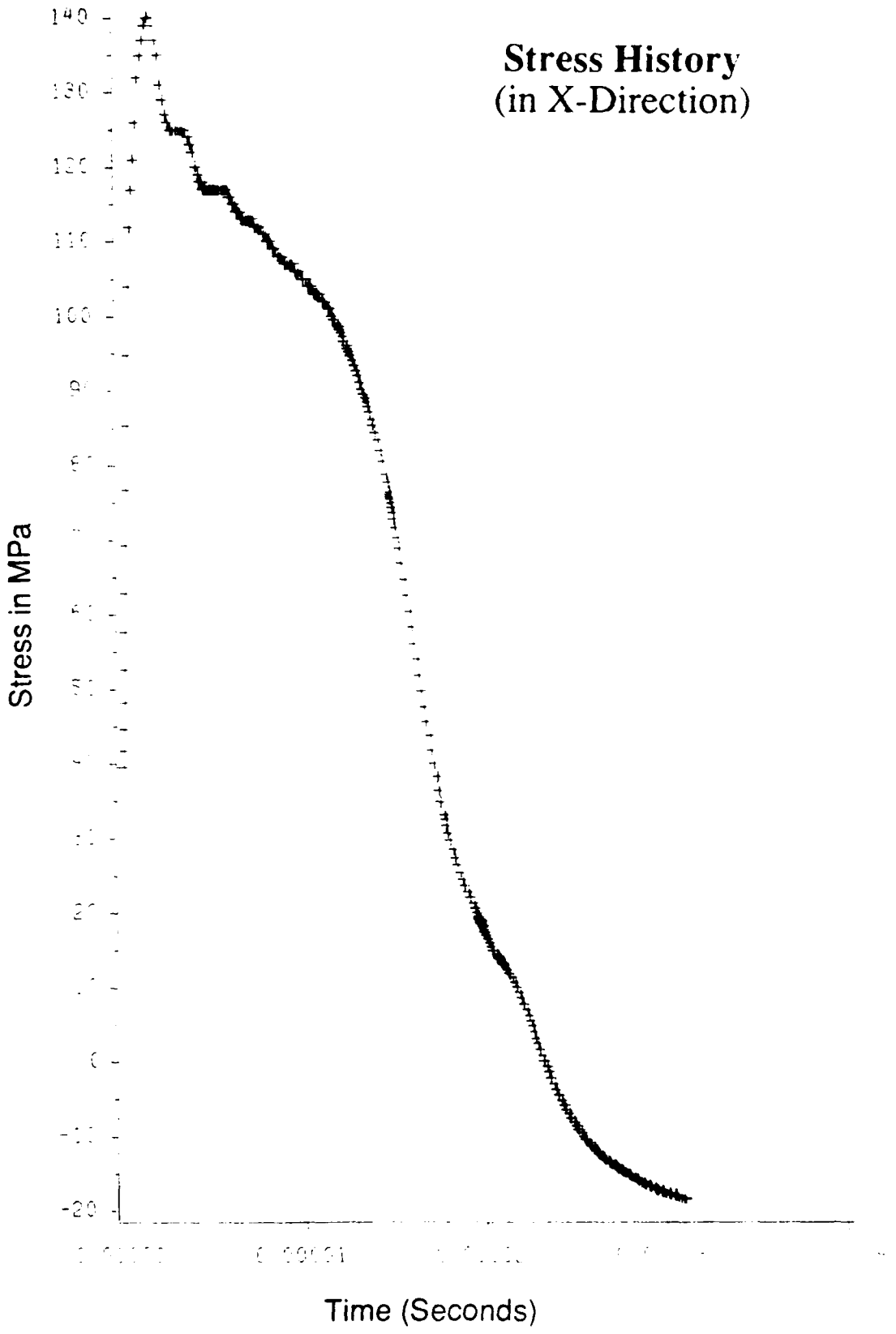

Figure 8. History of σ_{xx} at the Center of Interface Between Lexan and Aluminum Plates

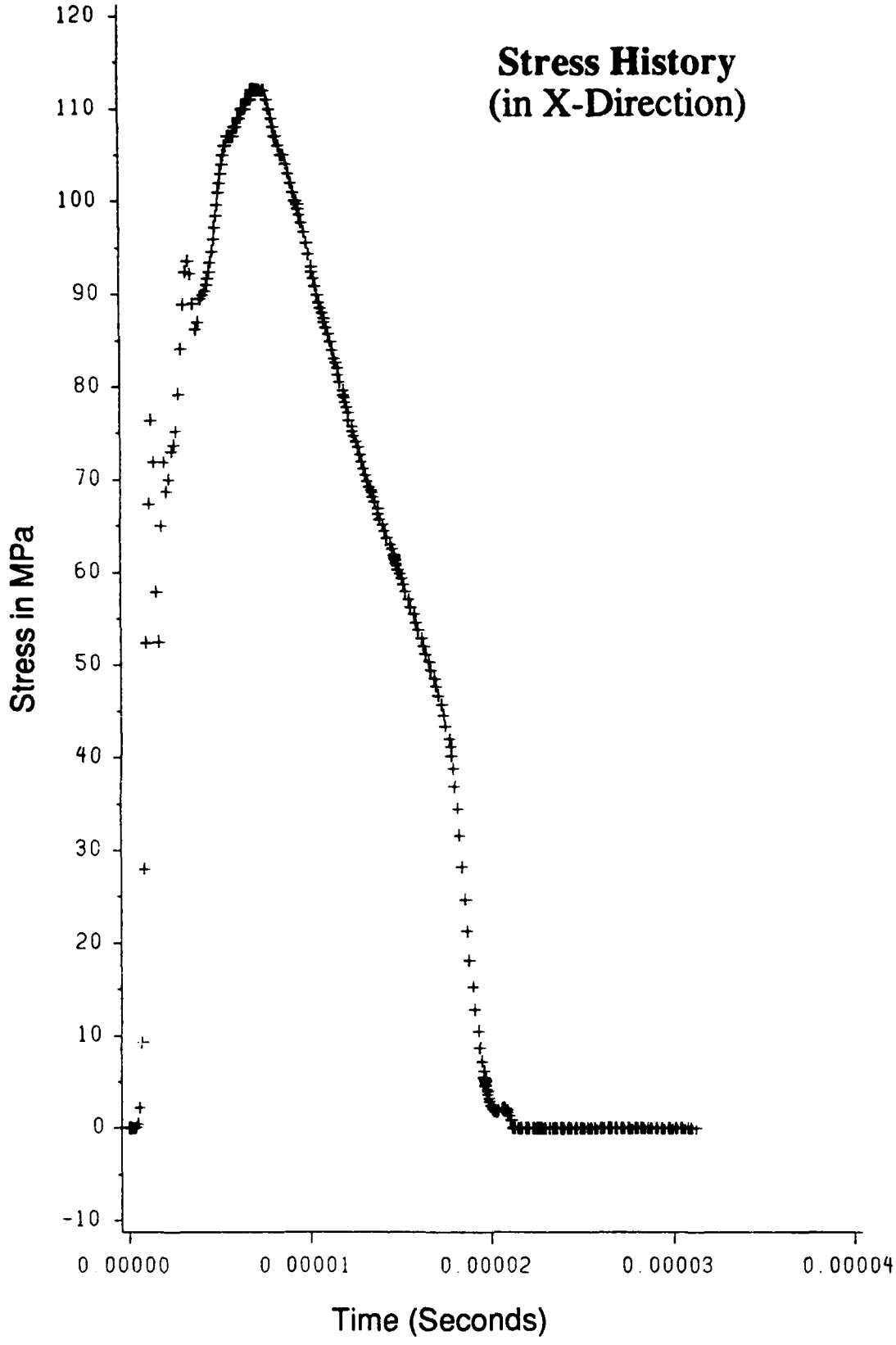

Figure 9. History of σ_{xx} at the Center of Interface Between Aluminum and Concrete Plates

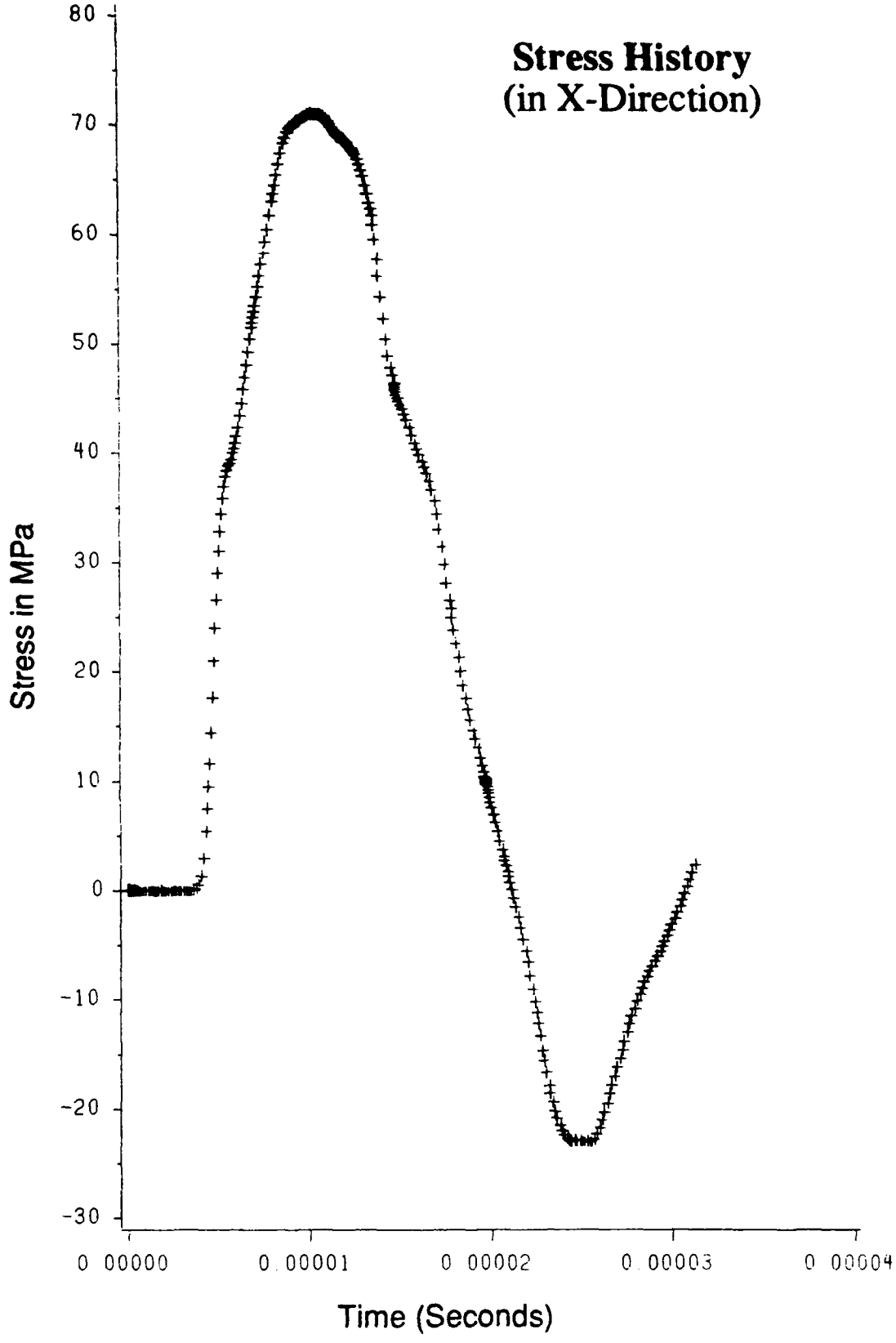

Figure 10. History of σ_{xx} at the Midpoint of Concrete

Figures 6 and 7 show the contour maps of normal stress in the longitudinal and transverse directions respectively. The progressive propagation of shock wave from the impacting interface is typical of wave propagation in two dimensions. However, the stress patterns in the thin aluminum plate rapidly become very complex because of wave reverberations between the two interfaces: Lexan®/aluminum and aluminum/concrete. Nevertheless, as shown in Figures 8 and 9, the stress history at each interface forms an expected simple "triangular" profile. Characteristic quantities of the loading profiles, e.g., peak stress and decay time are governed not only by two-dimensional wave interactions, but also such parameters as impact velocity, impact geometry, elastic constants, etc. The very early time oscillation in the history of normal stress at the second interface is a normal numerical artifact caused by a sudden increase in the rigidity of material, i.e., concrete.

The appearance of strong tension in the concrete slab at late times in Figures 6 and 10 is a well-understood phenomenon and was caused by the reflection of a triangular compression pulse from its back free surface. When the tensile stress exceeds the ultimate dynamic strength, a fracture occurs at that point. If the fracture extends over a wide region as shown in Figure 6, then a layer of material may even split away (spall) from the rest of the material. In localized loading, the spalled material often takes the shape of a cone because of the curvature in the wave front.

Unfortunately, since our fracture model does not describe the process of dynamic fracture (Reference 24), we cannot make a quantitative comparison of the calculations with the experimental results. But, there is a qualitative correlation between the triangular region of large tension found and the spalling observed in the test (see Figure 10 in Volume 1).

2. Shot M022

Calculations of Shot M022 are shown in Figures 10-13. The major goal of this test was to examine the influence of a sand layer on loading profiles and the modes of failure. However, in the simulation, the 11

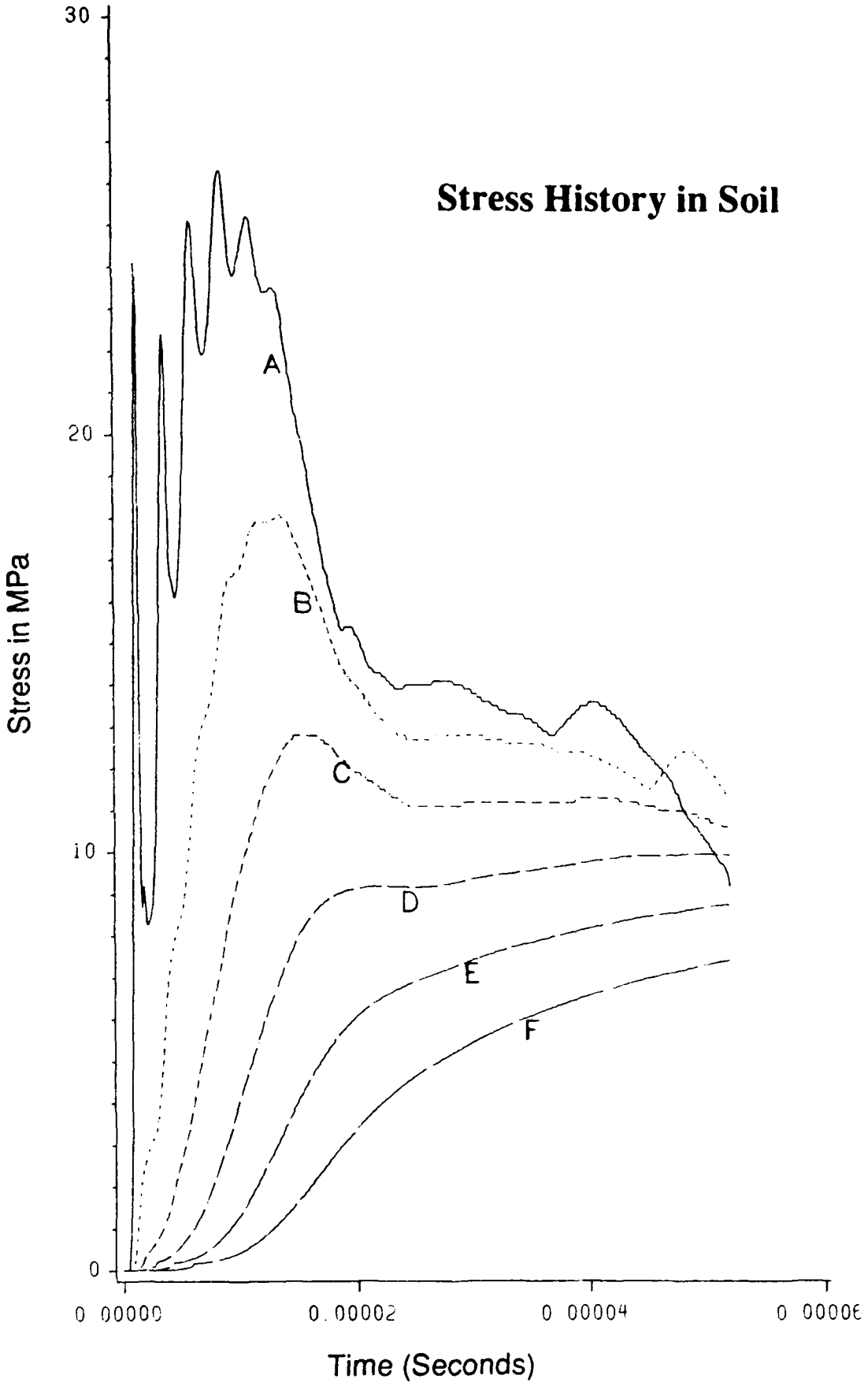

Figure 11. Attenuation and Dispersion of Ground-Shock Propagating in the Model Sand

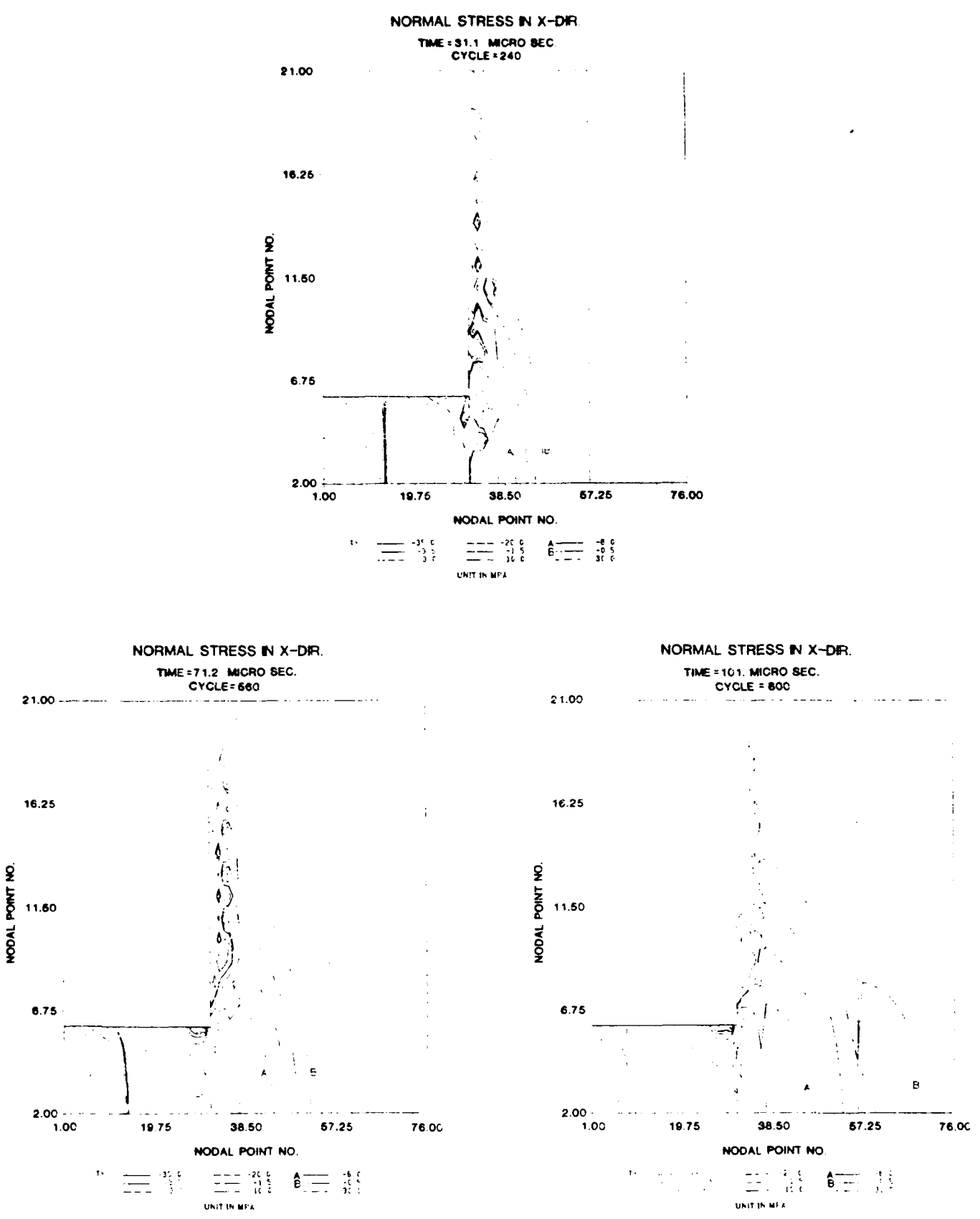

Figure 12. Temporal Evolution of Normal Stress (σ_{xx}) Distribution in the Longitudinal Cross Section of the Layered System with a Sand Layer

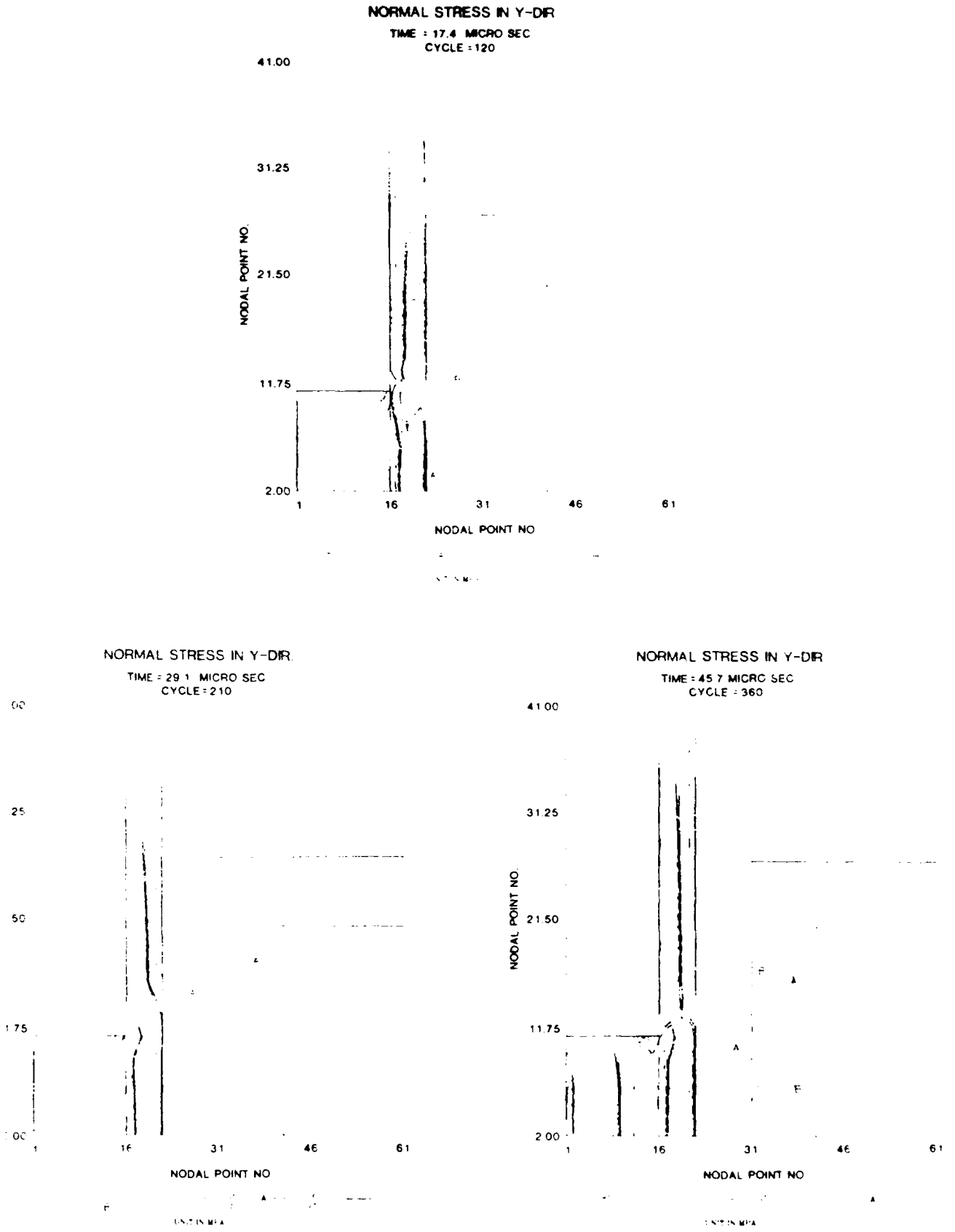

Figure 13. Temporal Evolution of Normal Stress (σ_{yy}) Distribution in the Longitudinal Cross Section of the Layered System with a Sand Layer

thickness of the sand layer was reduced from 3-inches to 1.18-inches (3 cm) to see wave propagation in the concrete plate within two hours of computing time on our IBM 370-168. This reduction was dictated soley by limited computing funds.

Characteristic features of wave propagation through the model sand layer are illustrated in Figure 11 in terms of the histories of the normal stress σ_{xx} at several successive points on the x-axis. Two noteworthy features of these histories are the rapid attenuation of peak stress and the dispersion of loading profile. In general, these features were generated by complex two-dimensional wave propagation through the model system. But, the most critical parameter is the slow wave speed in the model sand. In the pressure range of our interest (less than 5 kb) this speed is only about one- tenth of those in aluminum. This results in a strong lateral unloading of the foward-moving shock from the free surfaces of the projectile and the aluminum plate.

These histories indicate that by the time a wave reaches the surface of the concrete slab, the load is no longer a triangular shock pulse, but rather a step load having a time scale comparable to the fundamental period of the slab, or longer. The fundamental period calculated by use of the SAP IV program (Reference 25) was about 140 μsec. This means that the sand layer very effectively transforms a highly localized shock pulse into a long-time structural loading. Therefore, if there were any failure in the slab it will be one of the structural modes such as bending. Figures 12 and 13 show another view of the above described transformation in terms of stress contours.

Although the wave calculation was not carried out long enough to observe a tensile failure caused by bending, a bending failure consistent with the calculation was observed in the specimen recovered after the test.

One additional conclusion that can be drawn from the above described results is that the wave analysis of the scale model testing is an effective means of investigating both early-time stress wave response and

"late-time" structural response in a unified fashion by directly focusing on shock waves that excite the layered system. We will illustrate this advantage in the next example.

B. A BURIED MODEL FRAME

The goal of this exercise was to demonstrate the potential use of the program to analyze a more complex model than a plane slab. Of particular interest was the applicability of the program for investigating intermediate or "long-time" structural response in a model structure subjected to a shock loading.

The geometry of the problem we considered is shown in Figure 14. It is essentially Shot M022, but modified so that the model structure is situated in a more realistic environment. However, the selection of dimensions was influenced by external factors such as the cost of computing time and the size of the current program. The soil layer was further reduced to 1 cm.

Since early time responses are similar to those found for Shot M022, only late time stress contours were analyzed to focus on structural response result from a stress pulse propagated through a layer of protective soil.

Figures 15 and 16 show the distributions of normal stress at three successive stages of wave propagation. Complex profiles in the aluminum plate and simple wave profiles in the soil layer were very similar to those found for Shot M022. In spite of a relatively thin soil layer, there was a subtantial attenuation and dispersion of waves caused mostly by lateral unloading. As in the case of M022, the unloading was determined by the wave speed in soil which is an order of magnitude slower than those in aluminum and Lexan®. When the shock pulse reaches the concrete structure, it becomes a slowly varying load having time constants comparable to, if not longer than, the period of the first structural response mode. This load, in the first order approximation, is a distributed normal thrust.

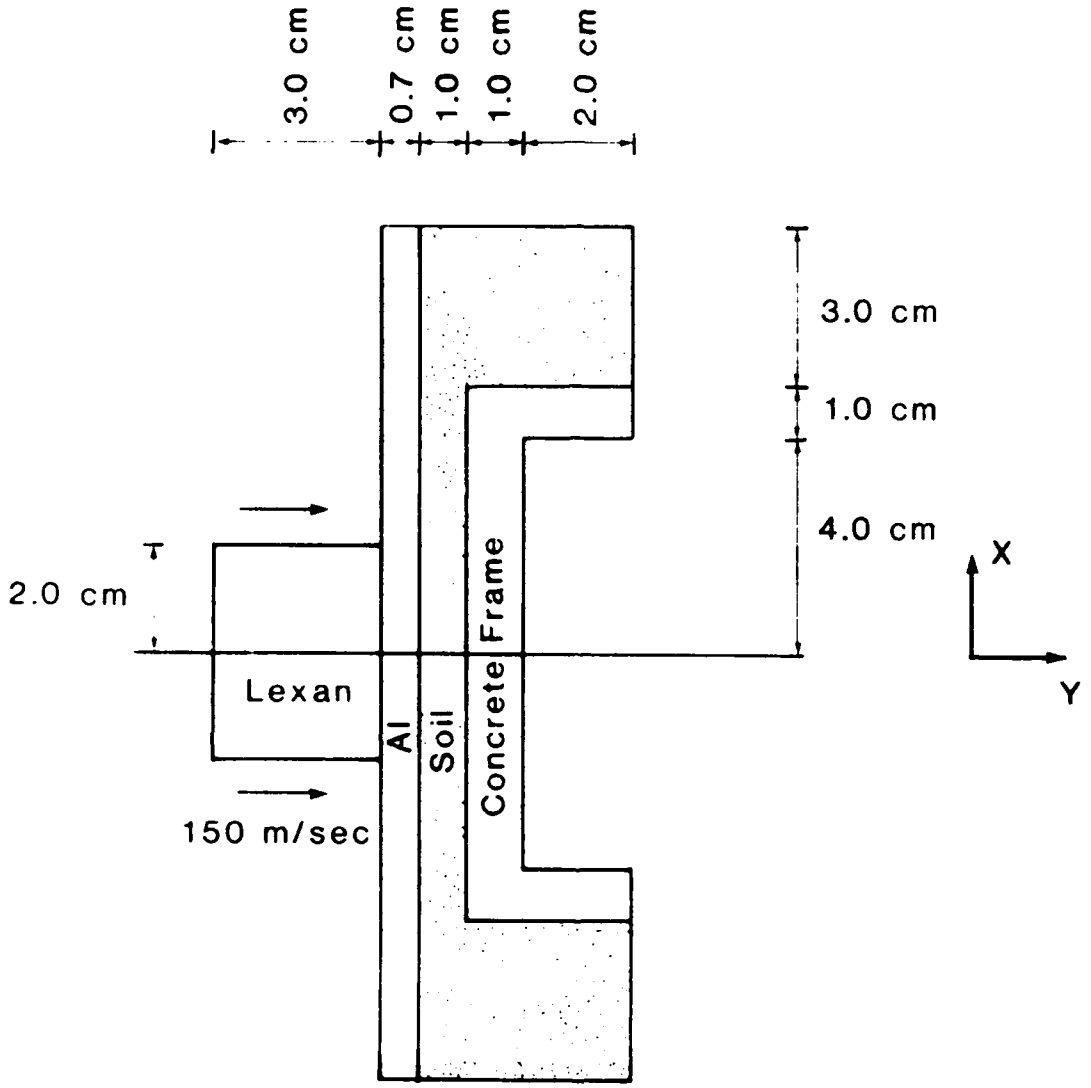

Figure 14. The Geometry of a Buried Model Frame Used for Calculation

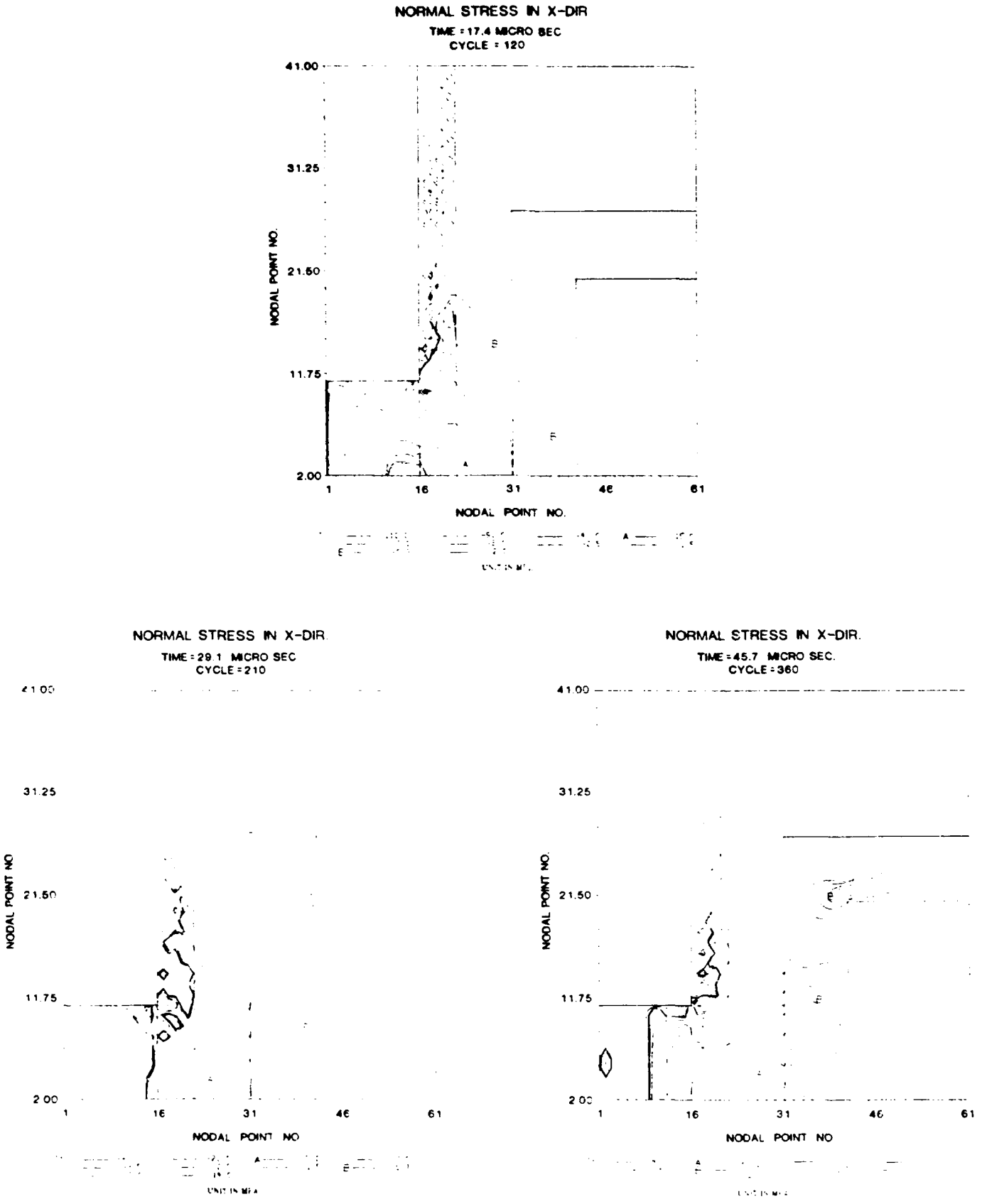

Figure 15. Temporal Evolution of Normal Stress (σ_{xx}) Distribution in a Layered System Shown in Figure 14

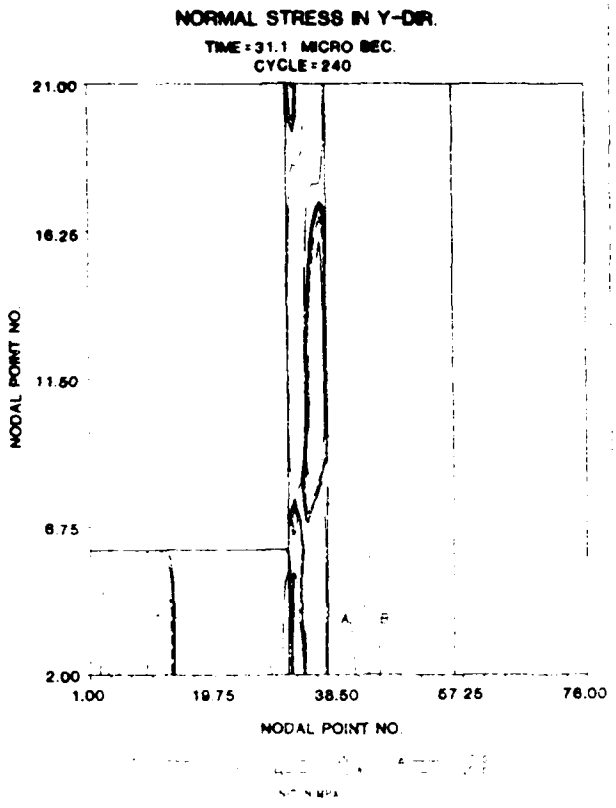

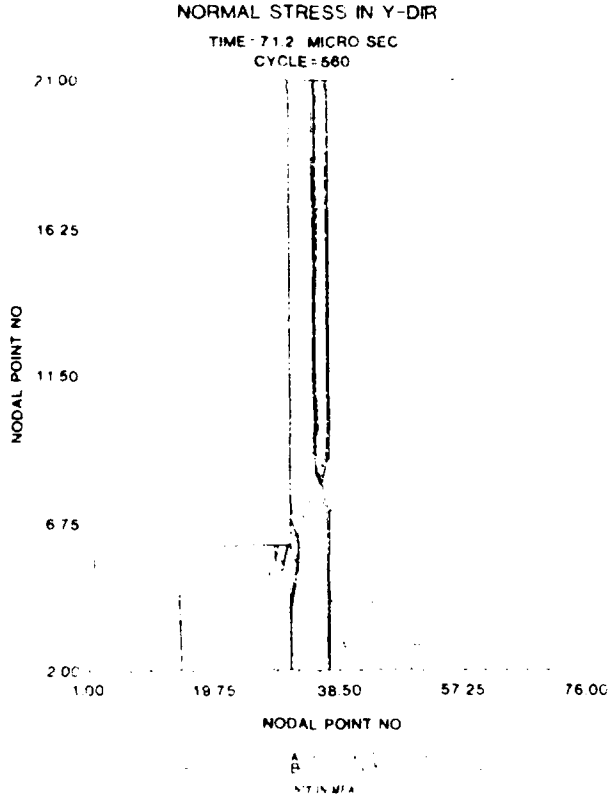

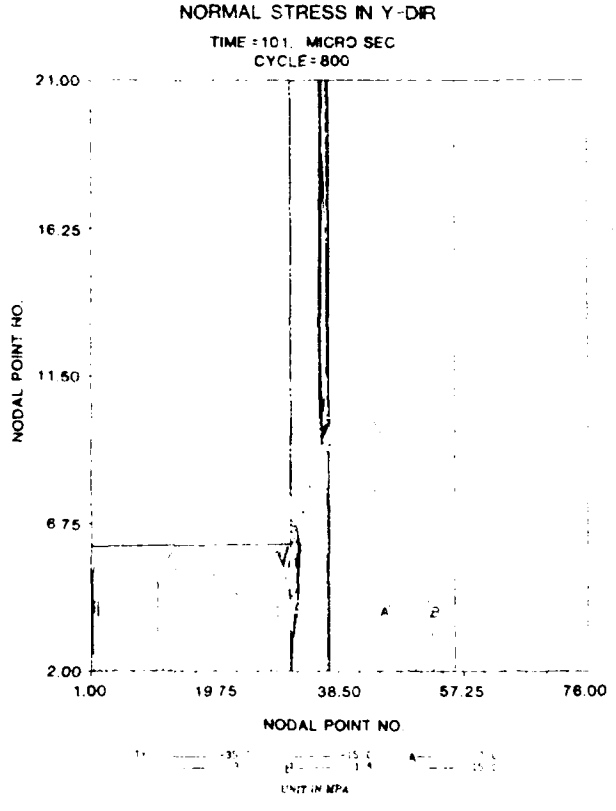

Figure 16. Temporal Evolution of Normal Stress (σ_{yy}) Distribution in a Layered System Shown in Figure 14

Therefore, if the frame is excited in a simple structural mode, the mode can be identified by examining the pattern of stress distribution. For instance, it is believed that the patterns of tension and compression at 45.7 μsec (last contour maps) correspond to the shape of the fourth fundamental mode (symmetric bending mode) of the frame shown. The alternating pattern of tension and compression in Figure 16 and the corresponding compression regions in Figure 15 are exactly what is expected from such a bending response. The period of the fourth mode, according to the SAP IV program, was about 53 μsec. However, no attempt was made to obtain a quantitative comparison because of the difficulty in duplicating the identical dynamic load for the SAP program.

Nevertheless, an important conclusion of this calculation is that model testing combined with numerical simulation is a cost effective means of generating data base for analysis and aid in the design of protective structures under close-in detonations.

SECTION IV

CONCLUSIONS

In the foregoing, we described (1) the successful development of a two-dimensional Lagrangian finite difference code for the wave analysis of the scale model testing of buried structures under dynamic loading and (2) the development of constitutive relations for the description of porous materials such as soil and concrete. We considered three sample calculations involving concrete slabs representing actual test configurations and a buried model frame. Results of the former agreed with the test results regarding failure modes, and provided a rational basis for interpreting them in terms of load profiles at concrete structures.

Some of the advantages of the wave approach are:

- regimes of both stress-wave response and early structural response can be analyzed in a unified scheme

- the analysis directly focus on the stress waves that excite structures as well as shock-transmitting layers

Other noteworthy features of the results are:

- for the configurations tested here the slow wavespeed in sand layers is the major cause for the attenuation and dispersion of ground shock that changed the mode of failure from spalling to a structural failure by bending.

- an aluminum plate, because of its fast wavespeed relative to sand, made an effective layer of spreading loads over a wider area of sand. This phenomenon may be of some interest in the design of protective structures by using the concept of layered systems.

REFERENCES

1. Crawford, R.E., Higgins, C.J., and Bultman, E.H., The Air Force Manual for Design and Analysis of Hardened Structures, AFWL-TR-74-102, Air Force Weapons Laboratory, Kirtland Air Force Base, Albuquerque, NM, October 1974.

2. Fundamental of Protective Design for Conventional Weapons, The Department of the Army, Waterways Experimental Stations, Vicksburg, Mississippi, July 1984.

3. Hermann, W., editor, Materials Response to Ultra-High Loading Rates, National Materials Advisory Board Report NMAB-356, Washington, D.C., 1980.

4. Nelson, I., "Numerical Solution of Problems Involving Explosive Loading," in Proc. of Dynamic Methods in Soil and Rock Mechanics, Vol. 2, Balkena, Rotterdam, 1977.

5. Ross, C.A., editor, Proc. of Symposium on the Interaction of Non-Nuclear Munition with Structures, U. S. Air Force Academy, Colorado, May 10-13, 1983, University of Florida Graduate Engineering Center, Eglin AFB, FL 1983.

6. Ross, C.A., and Thompson, P. Y., editors, Proc. of the Second Symposium on the Interaction of Non-Nuclear Munition with Structures, Panama City Beach, FL, April 15-18, 1985, University of Florida Graduate Engineering Center, Eglin AFB, FL, 1985.

7. Zukas, J., et al., Impact Dynamics, John Wiley & Sons, New York, 1982.

8. Wilkins, M., "Calculation of Elastic-Plastic Flow," in Methods of Computational Physics, Vol. 3, B. Alder, editor, Academic Press, New York, 1964.

9. Swegle, J.W., "TOODY-IV-A Computer Program for Two-Dimensional Wave Propagation," SAND-78-0552, Sandia National Laboratories, Albuquérque, NM, September 1978.

10. Hoffmann, R., "SEALTH, A Lagrangian Explicit Finite Difference Code for Solids, Structural, and Thermohydrolic Analysis," EPRI NP-260, Science Applications Inc., for Electric Power Research Institute, Palo Alto, CA, August 1976.

11. Seaman, L., "TROTT Computer Program for Two-Dimensional Stress Wave Propagation," Contract Report ARBRL-CR-00428, SRI International, Menlo Park, CA, April 1980.

12. Hermann, W., "A Lagrangian Finite Difference Method for Two-Dimensional Motion Including Material Strength," AFWL-64-107, Air Force Weapons Laboratory, Albuquerque, NM, 1964.

13. Nilsson, L., "Impact Loading of Concrete Structures," Chalmers University of Technology, Department of Structural Mechanics, Publication 79:1, Goteborg, Denmark, 1979.

14. Desai, C.S., and Siriwardane, Constitutive Laws for Engineering Materials, Prentice Hall, New York, 1983.

15. Nelson, J., "Constitutive Models for Use in Numerical Computation," in Proc. of Dynamic Methods in Soil and Rock Mechanics, Balkena, Rotterdam, 1977.

16. Vermeer, P.A., and Luger, H.J., Deformation & Failure of Granular Materials, Balkena, Rotterdam, 1982.

17. Baladi, G.Y., "An Elastic-Plastic Isotropic Constitutive Model for Sands," in Advances in the Mechanics & the Flow of Granular Materials, Vol. 2, M. Shahinpoor, editor, Trans Tech Publications, San Francisco, 1983.

18. Cowin, S.C., and Carroll, M.M., editors, The Effects of Voids on Material Deformation, AMD-Vol. 16, Am. Soc. Mech. Eng., New York 1976.

19. Swegle, J.W., "Constitutive Equation for Porous Materials with Strength," J. Appl. Phys., 51, 1980, pp. 2574-2580.

20. Horie, Y. and Park, J-K., "High Pressure Equation of State for Metal and Ceramic Powders," in Final Report of the DARPA Dynamic Materials Synthesis & Consolidation Program, Vol. 1, UCID-19663-85, Cline, C.F., editor, Lawrence Livermore Laboratory, Livermore, 1985.

21. Park, J-K., and Horie, Y., "Constitutive Equation for Geological Materials under High Dynamic Loading," in the proceedings cited in Reference 6.

22. Marsh, S.P., editor, LASL Shock Hugoniot Data, University of California Press, Berkeley, CA, 1980.

23. Charest, J.A., "Measurement of Stress Wave Characteristics in Selected Stemming Materials," TR 002, Dynasesn, Inc., Goleta, CA, 1977.

24. Curren, D. R., Seaman, L., and Shockey, D.A., "Dynamic Fracture of Solids," Physics Reports, Vol. 147, 1983, pp. 253-388.

25. Bathe, K-J., Wilson, E.L., and Peterson, F.E., SAP IV: A Structural Analysis Program for Static and Dynamic Response of Linear Systems, University of California, Berkeley, CA, 1974.

26. Drake, J.L., and Little, C.D., "Ground Shock from Penetrating Conventional Weapons," in the proceedings cited in Reference 5.

27. Sue, N.P., "A Yield Criterion for Materials," Inc. J. of Powder Metallurgy, 5, 1969, pp. 69-78.

28. Higgins, C.J., "Some Consideration in the Analysis and Prediction of

Ground Shock from Buried Conventional Weapons," in the proceedings cited in Reference 5.

(The reverse of this page is blank.)

APPENDIX A

GROUND SHOCK PROPAGATION IN VARIOUS SOIL TYPES

This appendix discusses the capability of the porous model to describe many different kinds of porous materials by appropriate choice of the functional forms. Presently, the model involves two critical functions that determine the inelastic behavior of porous materials. They are the P-α relationship and the yield function (see Section II.A). However, since the present P-α relationship is determined by a mechanistic model to minimize the number of free parameters, the function to be selected is only the yield function.

There are many suggestions for the yield function (some models involve more than one yield function) to describe the inelastic behavior of porous materials (Reference 15). In this study we chose a lemniscate function and evaluated the predictive capabilities of the model by conducting a parametric simulation of the scaled data on ground shock propagation in five soil types (Reference 26). These soils were characterized as: (1) loose density sand, (2) medium density sand, (3) very dense sand, (4) sandstone, and (5) silty sand. The shock data is said to be a compilation of more than one hundered explosion tests over the past 35 years.

The behaviors of the five soil types were modeled by appropriate selections of the material parameters in the lemniscate function illustrated in Figure A-1 and defined by

$$f = \left[(p + c_0) / A(\alpha)\right]^2 + \left[(3J_2)^{1/2} / B(\alpha)\right]^2 - \cos(\pi\theta / 2\phi) \qquad (A.1)$$

where

$$A(\alpha) = P_p(\alpha) - c_0 \qquad (A.2)$$

LEMNISCATE YEILD FUNCTION

$$g=\left(\frac{P+C_0}{A(\alpha)}\right)^2+\left(\frac{\sqrt{3J_0}}{B(\alpha)}\right)^2-\cos^n\left(\frac{\pi}{2}\,\frac{\theta}{\phi}\right)$$

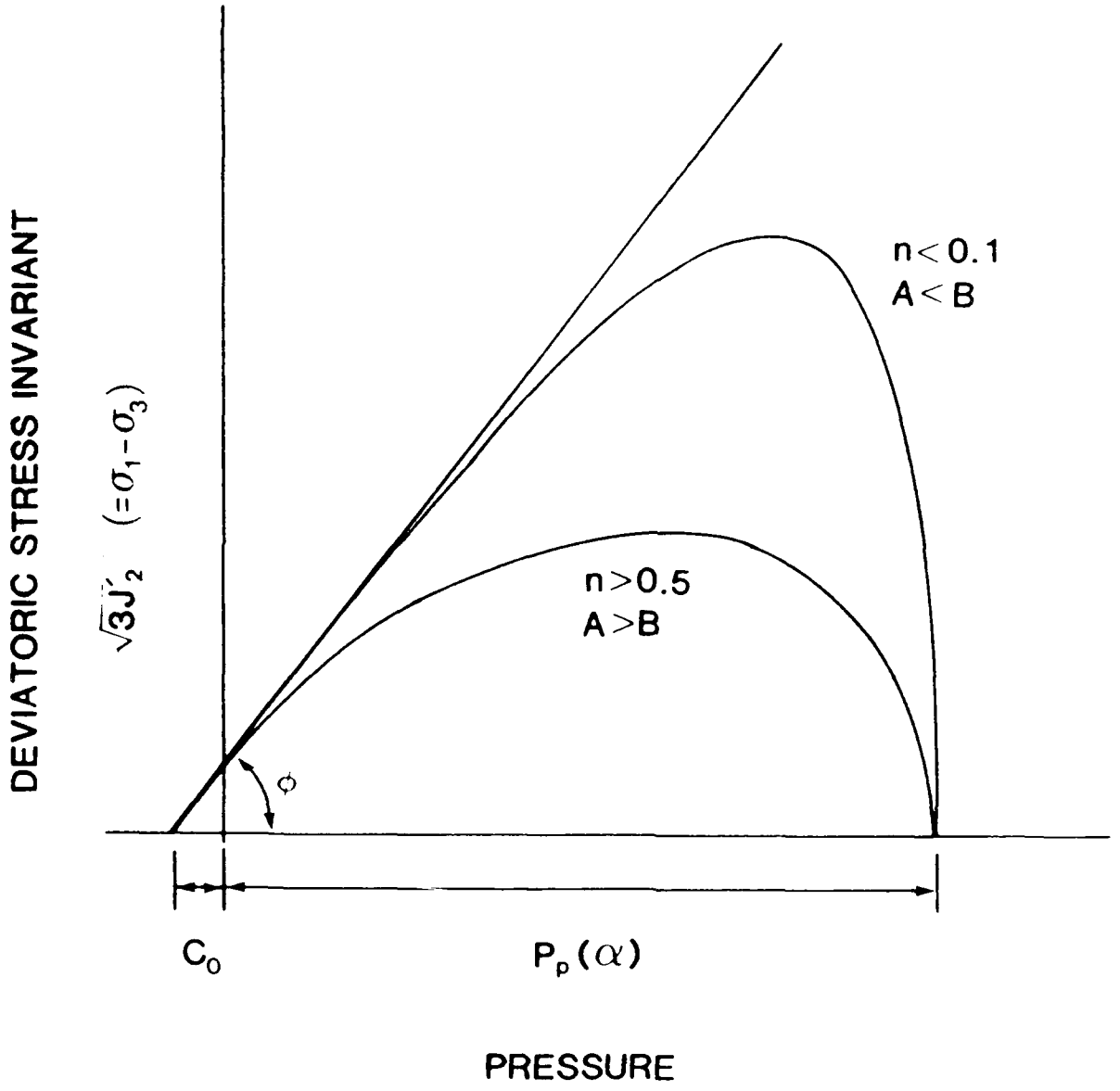

Figure A-1. Lemniscate Yield Function

$$B(\alpha) = c_m \cos^m(\pi\alpha / 2) \cdot A(\alpha) \qquad (A.3)$$

$$p_p(\alpha) = (Y/\beta) \left[(1-\alpha)^{-2\beta/3} - c_p(1 - \alpha_o)^{-2\beta/3}\right] \qquad (A.4)$$

c_o, c_m, m, β, and Y are constants.

The specific soil properties associated with the yield function are summarized in Table A-1. The relative importance of different parameters is difficult to determine, but four of them are found to govern characteristic features of the ground shock propagation in the five soil types. They are α_o (or the initial porosity that determines the sound speed ratio C_{to}/C_{so}, n and C_m that control the maximum shear strength as illustrated in Figure A-1, and ϕ that determines the initial slope of the yield function. In Suh's formulation (Reference 27), ϕ is the slope of the Mohr-Coulomb failure surface.

Other material properties that are associated with the Mie-Grüneisen equation for the solid components of these soils are assumed to be the same for all the soil types and are listed in Table A-2.

The parametric simulations of buried explosions were conducted by using the gas expansion model developed by Chadwich et al. in Reference 28 . In this model the pressure of the exploding cavity is given by

$$p = \dot{p}_o(a/a_o)^{-3r} \qquad (A.5)$$

where p_o is the initial pressure when the cavity radius was a_o, a the current radius, and r a constant. The explosive parameters were obtained from References 28 and 29 and are summarized in Table A.3. Selected results of the simulations are shown in Figures A-2 - A-5 and Table A-4. In these calculations, however, no systematic attempt was made to optimize the materials properties to obtain the best fitting to the experimental results.

TABLE A-1. PARAMETERS OF THE LEMNISCATE YIELD FUNCTION

Parameters	loose sand	medium sand	dense sand	sand stone	silty sand
α_o	0.5	0.59	0.68	0.78	0.78
n	0.05	0.05	0.05	0.05	0.5
ϕ(degree)	53	53	53	53	45
C_o(MPa)	0.1	0.1	0.1	0.1	0.5
C_m	7.2	6	3	1	1
m	1.2	1.2	1.2	1.2	1.2
Y(MPa)	2	2	2	2	2
β	6	6	6	6	6
C_p	0.95	0.95	0.95	0.95	0.95

TABLE A-2. EQUATION OF STATE*

Properties	loose sand	medium sand	dense sand	sand stone	silty sand
Initial porosity (%)	50	41	32	22	22
Sound-speed ratio (C_{to}/C_{so})	0.05	0.08	0.15	0.2	0.2
Density of Solid (kg/m^3)	2700	2700	2700	2700	2700
Shear modulus (Solid)(GPa)	24	24	24	24	24
Bulk modulus (Solid)(GPa)	39	39	39	39	39

*The pressure-volume equation for solid:

$$p_s(\alpha) = 39 \left(\frac{V_s}{V_{so}} - 1\right) + 60.5 \left(\frac{V_s}{V_{so}} - 1\right)^2 , \text{ in GPa}$$

TABLE A-3. EXPLOSIVE PARAMETERS

Explosive type:	TNT
Charge Weight, L:	512 kg
Radius of cavity, a_o:	42 cm
Boundary pressure, P_o:	22 Gpa
The constant, r:	2.33
Scaled range W:	1 m/kg$^{1/3}$ = 8 m

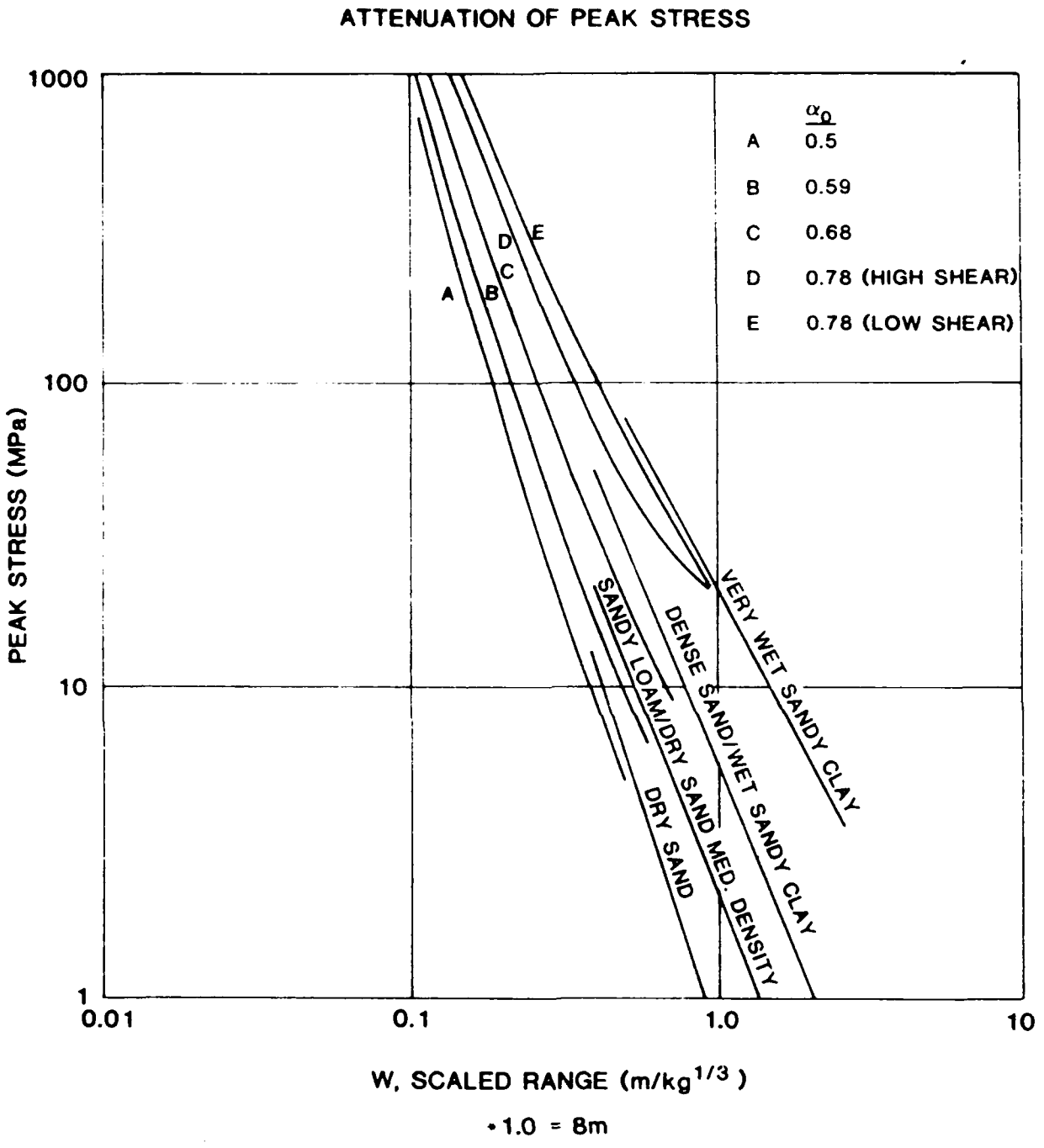

Figure A-2. Attentuation of Peak Stress in Various Sands. Lower Curves Represent Summary of the Experimental Data. The Bending of Curve D at About 50 MPa Was Caused by a Too High Shear Strength in the P-α Equation

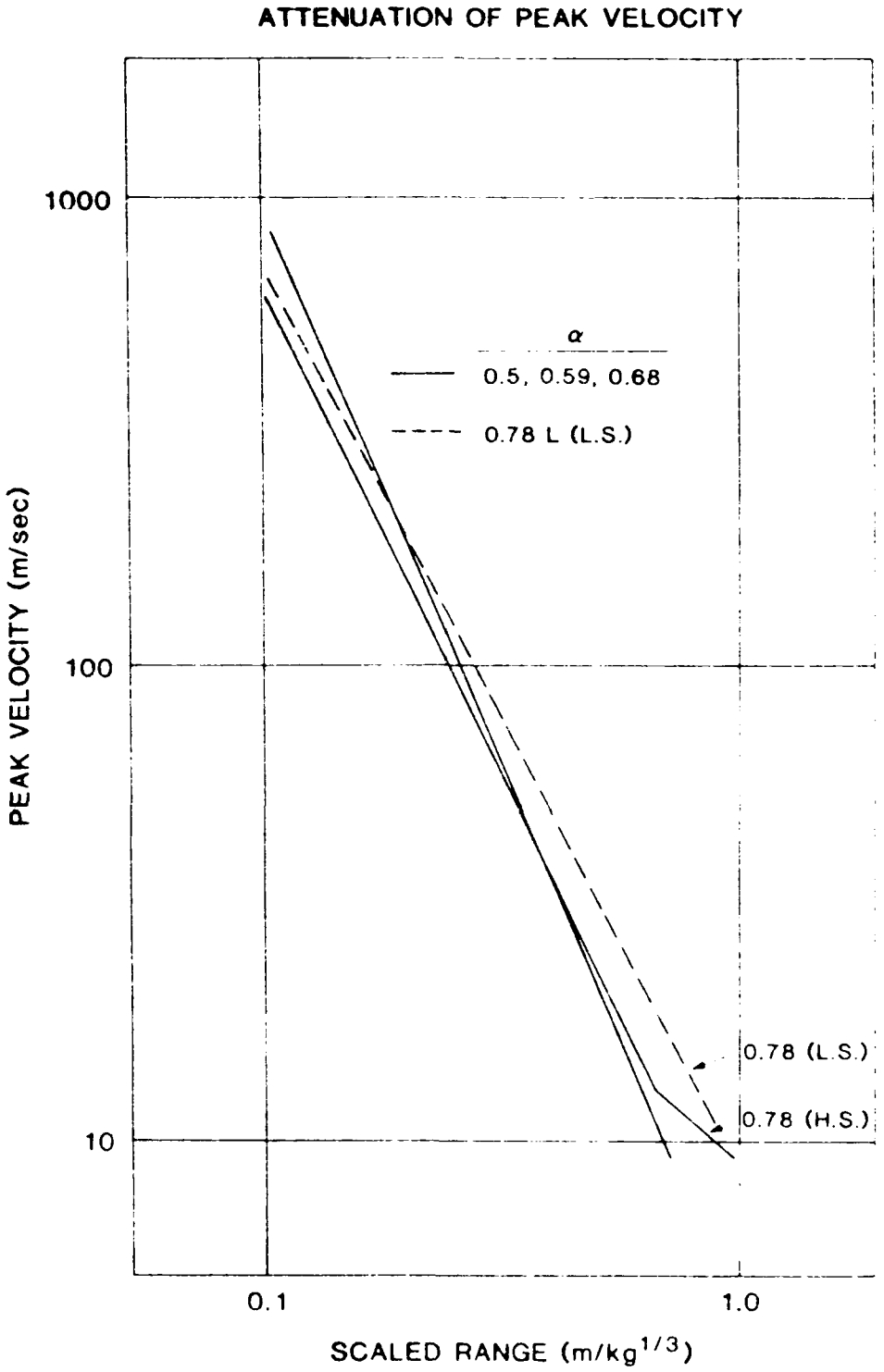

Figure A-3. Attenuation of Peak Particle Velocity. For Clarity Experimental Curves Were Not Drawn, But Were Located Between the Calculated Single Line for α = 0.5, 0.59, and the Line for α = .78 (L.S.). Again the Bending of the Line for α = .78 (H.S.) Was Caused by a Too High Shear Strength in the [illegible] Model

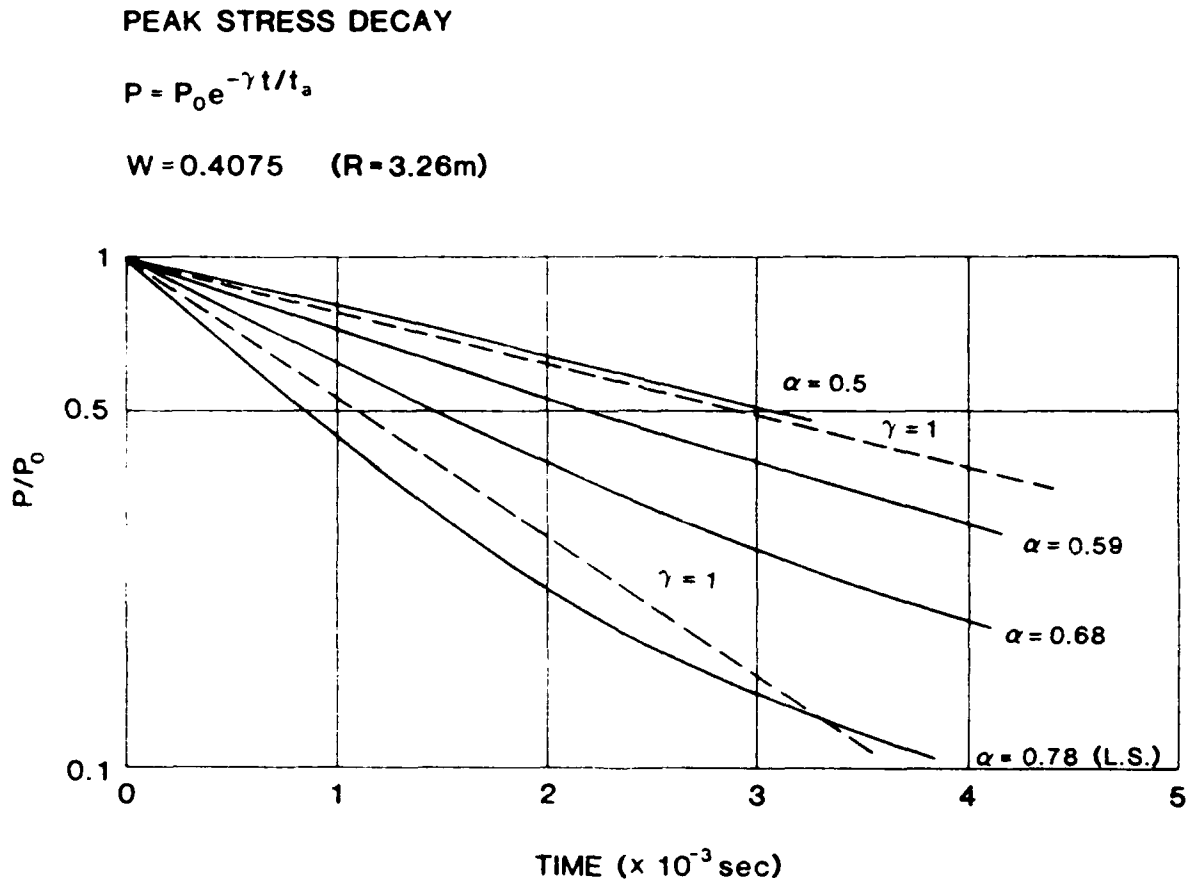

Figure A-4. Peak Stress Decay in Time at a Fixed Stand-Off Distance. Experimental Data are Only Shown for α = .78 (L.S.) by Broken Lines

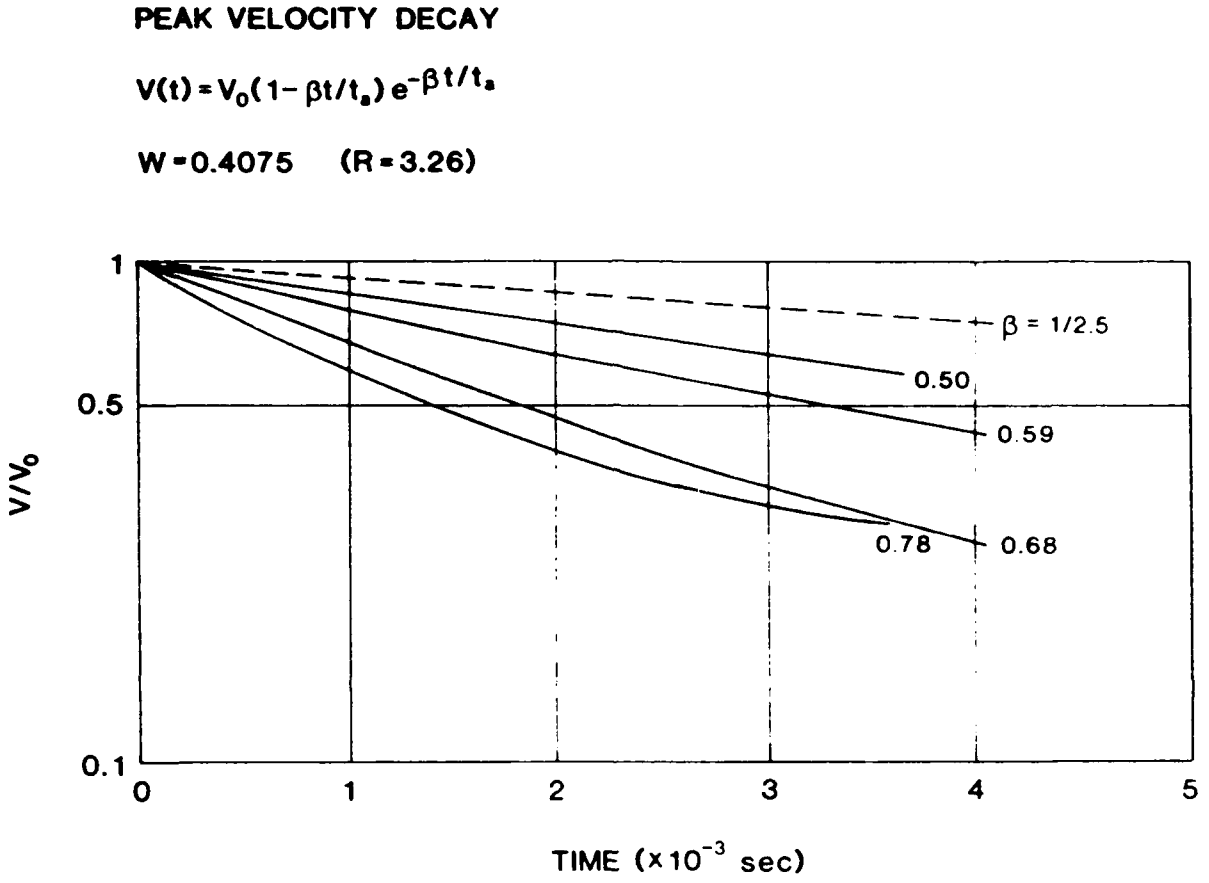

Figure A-5. Peak Velocity Decay in Time at a Fixed Stand-Off Distance. There was no Agreement Found Between Calculations and Experimental Results

TABLE A-4. CALCULATED ATTENTUATION COEFFICIENT, n

Sand Type	Initial α_o	Peak Stress Level (MPa)	n
Loose sand	0.50	1000 - 30	3.52
		30 - 5	2.80
Medium dense sand	0.59	1000 - 60	3.31
		60 - 7	2.53
Dense sand	0.68	1000 - 60	3.00
		60 - 10	2.23
Sand stone (High shear strength)	0.78	1000 - 100	2.44
		100 - 35	2.05
		35 - 20	1.05
Silty sand (low shear strength)	0.78	1000 - 80	2.33
		80 - 20	1.68

Figure A-2 shows a comparision of calculated attenuation rates of peak stress with those summarized from the experimental data. The calculated trend of the attenuation rates is in agreement with that discussed in Reference 26, involving parameters such as porosity and seismic speed.

A similar agreement is found with the results regarding other parameters: attenuation coefficients (Table A-4), attenuation rates of peak particle velocity (Figure A-2), and stress decay (Figure A-3). However, no good correlation was obtained with particle velocity decay (Figure A-4). In

these figures, the stress and velocity decays that characterize pulse profiles are defined by Drake and Little as follows (Reference 26). First, the arrival time t_a is defined by

$$t_a = R/c \tag{A.6}$$

where R is the distance from the explosion and c is the seismic wave propagation velocity. Then, the stress and velocity decays are defined by

$$\sigma(t) = p_o \exp(-\gamma t/t_a) \tag{A.7}$$

$$v(t) = v_o(1 - \beta t/t_a) \exp(-\beta t/t_a) \tag{A.8}$$

where σ_p and v_p are the values of the peak stress and peak particle velocity and γ and β are time constants. They find that for most applications these time constants may be approximated by $\gamma = 1.0$ and $\beta = 1/2.5$.

They also found that the rise time of these wave forms is typically about one/tenth of the travel time to the target point. The corresponding calculated results varied from 0.06 to 0.17 depending upon soil types and locations. An accurate evaluation of the coefficient is difficult because of the ambiguity in the definition of travel time for a dispersed wave profile. But, the calculated results are consistent with the reported empirical value.

APPENDIX B

INPUT PREPARATION

Four sets of input data are required to run a problem. They are, in the order of appearance, general running data, materials data, cell and coordinate layout data, and velocity data. As an example the complete input deck for the calculation of the buried frame is shown in Figure B-1. Any consistent system of units can be used for the calculations. Some popular systems are shown in Figure B-2 (Reference 9).

A. RUNNING DATA

Line 1 (2I5, F10.0)

Columns	Variable
1 - 5	frequency in cycles for printing selected solutions
6 - 10	the maximum number of computing cycles
11 - 20	initial time increment

Line 2 (5I5)

Columns	Variable
1 - 5	boundary condition

-1 = Fixed y-velocity at $i = i_{min}$ and i_{max}
-2 = Fixed y-velocity at $i = i_{min}$ only
-3 = All free edges
-4 = Fixed y-velocity at $i = i_{min}$,
Fixed x-velocity at $j = j_{min}$ and j_{max}
-5 = Fixed y-velocity at $i = i_{min}$ and i,
Fixed x-velocity at $j = j_{min}$.

6 - 10	number of blocks in the problem
11 - 15	number of materials

```
 30   450    .1E-06                                                    ] General
 -2     7    4    1                                                   ] running
.3470E+11                                                             ] data

119 E+01      .689E08      .904E10      .198E06      5                 ]
  4.          .1           0.02                                       ]
 300000.                                                              ]
.800  E12                                                             ]
 .278 E01     .750E09      .300E12      .650E06                       ]
  4.          .1           0.02                                       ] Materials
 3.900E11     6.05E11                                 1                ] data
 2.7          7.5  E08     2.40E11   512799.                          ]
  4.          .1           0.02                                       ]
  .08         .59                                                     ]
  .131E12                                                             ]
 .208E01      .282E09      .940E11      .351E06                       ]
 4.           .1           0.02                                       ]

  1    15    0.           2.8          2.8          0.          1     ]
  1    11    0.0          0.0          2.0          2.0               ]
 15    16    2.8          3.0          3.0          2.8         1     ]
  1    11    0.0          0.0          2.0          2.0               ]
 16    21    3.0          3.7          3.7          3.0         2     ]
  1    41    0.           0.           8.0          8.0               ] Cell and
 21    31    3.7          4.7          4.7          3.7         3     ] coordinate
  1    41    0.           0.           8.0          8.0               ] layout
 31    61    4.7          7.7          7.7          4.7         3     ]
 26    41    5.0          5.0          8.0          8.0               ]
 31    61    4.7          7.7          7.7          4.7         4     ]
 21    26    4.0          4.0          5.0          5.0               ]
 31    41    4.7          5.7          5.7          4.7         4     ]
  1    21    0.0          0.0          4.0          4.0               ]

  3    11    16       15000.                                          ] Velocity data
```

Figure B-1. Input Data for the Calculation of the Buried Frame Shown in Figure 14

Sets of Units

Quantity	c.g.s.	c.g. μs	S. I.	f.p.s.
Time	s	μs	s	s
Length	cm	cm	m	ft
Mass	gm	gm	kg	slug
Force	dyn	T dyn	Newton	lb
Energy	erg	T erg	Joule	ft.lb
Energy Density	erg/gm	Mbar cm^3/gm	J/kg	ft.lb/slug
Power	erg/s	T erg/s	Watt	ft.lb/s
Density	gm/cm^3	gm/cm^3	kg/m^3	$slug/ft^3$
Pressure	dyn/cm^2	Mbar	Pa	lb/ft^2

Figure B-2. Consistent Systems of Units That Can Be Used for Code Calculations

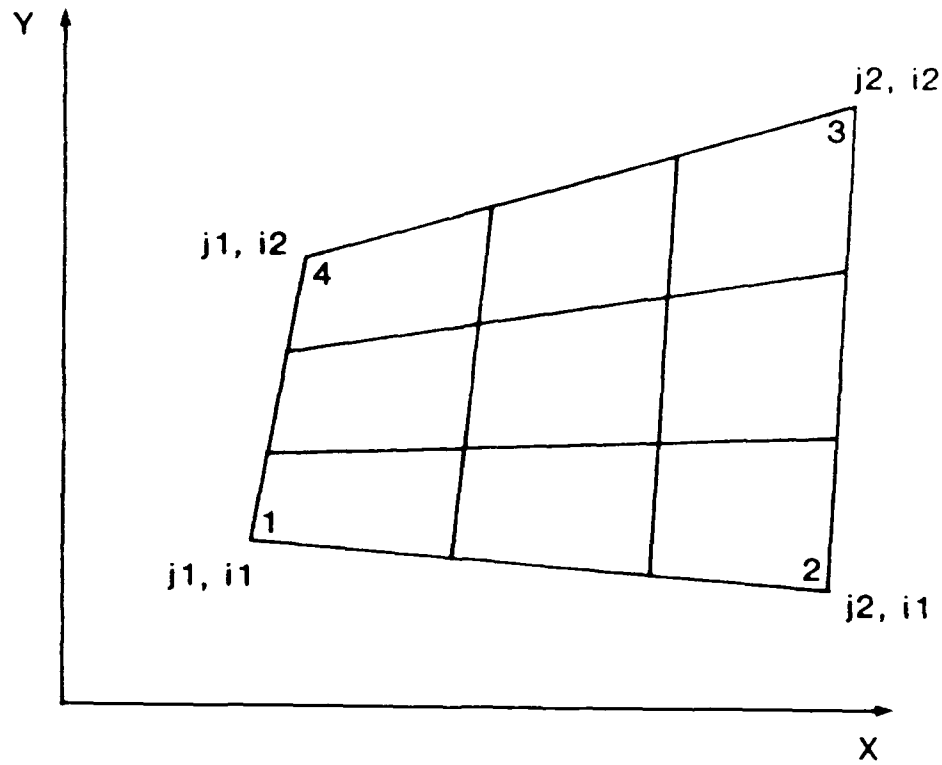

Figure B-3. Definition of Lagrangian Positions in a Quadilateral Block

16-20	velocity initialization 1 = velocity initialized for all i up to an interface j value for a projectile impact -1 = velocity initialized for all i and j from an interface value to j_{max}.
21 - 25	maximum value of j in initial calculations.

B. MATERIAL DATA

Line 1 (4F10.0, I5)

Columns	Variables
1 - 10	a_1 in Equation (14)
11 - 20	a_2 in Equation (14)
21 - 30	a_3 in Equation (14)
31 - 40	Γ in Equation (14)
41 - 45	1 = porous material

Line 2 (4F10.0, I5)

Columns	Variables
1 - 10	specific density
11 - 20	yield stress
21 - 30	shear modulus
31 - 40	longitudinal sound speed
41 - 45	fracture indicator 5 = fracture in the x-direction 6 = fracture in the y-direction

Line 3 (3F10.0)

Columns	Variables
1 - 10	quadratic viscosity constant
11 - 20	linear viscosity constant
21 - 30	triangle viscosity constant

Line 4 (2F10.0)

Columns	Variables
1 - 10	C_{to} / C_{so} = sound speed of porous material / sound speed of its solid component
11 - 20	α_o

Line 5 (F10.0) skip this line if the fracture is not considered.

Columns	Variables
1 - 10	fracture strength

Repeat Line 1-5 as many times as the number of materials in the problem.

C. GRID LAYOUT DATA

Line 1 (2I5, 4F10.0, I5)

Columns	Variables
1 - 5	j1
6 - 10	j2
11 - 20	XA(1)
21 - 30	XA(2)
31 - 40	XA(3)
41 - 50	XA(4)
51 - 55	material number

where j1 and j2 define Lagrangian x-positions of a quadrilateral block as shown in Figure B.3. XA(n) are x-coordinates of the corners of the block read in counterclockwise direction starting with pint of smallest j, i values.

Line 2 (2I5, 4F10.0)

Columns	Variables
1 - 5	i1
6 - 10	i2
11 - 20	YA(1)
21 - 30	YA(2)
31 - 40	YA(3)
41 - 50	YA(4)

where i1 and i2 are Lagrangian y-positions defined in Figure B-2 and YA(n) are y-coordinates of the corners of the quadrilateral block.

C. VELOCITY DATA

Line 1 (3I5, F10.0)

Columns	Variables
1 - 5	minimum i value initialized at the velocity u
6 - 10	maximum i value initialized at the velocity u
11 - 15	interface j value for a projectile impact
16 - 25	initial velocity of a projectile

(~~The reverse of this page is blank.~~)

APPENDIX C

LISTING OF COMPUTER PROGRAMS

```
      IMPLICIT REAL*8(A-H,O-Z)
      COMMON/T/X(3000),Y(3000),XD(3000),YD(3000),H(3000),A(3000)
     *,Z(3000),D(3000),SXX(3000),SYY(3000),SZZ(3000),TXY(3000)
     *,TXX(3000),TYY(3000),TZZ(3000),P(3000),E(3000),YY(3000),
     *EVV(3000),EXX(3000),EYY(3000),EZZ(3000),EXY(3000),ALP(3000),
     *IH(3000)
      COMMON/EQS/EQSTC(6),EQSTD(6),EQSTS(6),RHO(6),YC(6),UMU(6)
     *,CLIN(6),C_SQ(6),TEIQ(6),SP(6),EQSTG(6)
      COMMON/GEN/UZERO,DT,DTN,DTM,IJBUND,JMAX,JMIN,KMAX,KMIN,KCHEK
      COMMON/IND/ NPE(10)
      COMMON/PSR/ TSR(10)
      COMMON/POR/ ALP(3000),SXXS(3000),SYYS(3000),SZZS(3000),TXXS(3000)
     *,TYYS(3000),TZZS(3000),TXYS(3000),PS(3000),EVVS(3000),EXXS(3000)
     *,EYYS(3000),EZZS(3000),EXYS(3000),EJ(3000),ALPO(6),IPOR(6),CTCS(6)
      DIMENSION XL(100,100),YL(100,100),MM(100,100),LVAR(100,100)
C
      JSIZE=15000
      JXX=100
      KXX=100
C
      READ(1,2222) NN,NMAX,DT
 2222 FORMAT(2I5,E10.3)
      WRITE(3,2223) NN,NMAX,DT
 2223 FORMAT(1X,'NN=',I3,3X,'NMAX=',I5,3X,'DT=',E12.5)
C
C
      CALL LAYOUT(JSIZE,JXX,KXX,XL,YL,MM,LVAR)
C
      TIME=0.
      DTN=DT
      N=0
      NNN=NN
  100 N=N+1
      IF(N.GT.NMAX) CALL EXIT
C
      CALL SWEEP(JSIZE,JXX,KXX,XL,YL,MM,LVAR)
C
      LV1=LVAR(11,2)
      LV2=LVAR(16,2)
      LV3=LVAR(21,2)
      LV4=LVAR(26,2)
      LV5=LVAR(31, 2)
C
      TIME=TIME+DT
CCC   WRITE(3,1031) N,TIME,P(LV1),EVV(LV1),ALP(LV1),SXX(LV1)
CCC  *,SYY(LV1),P(LV2),EVV(LV2),ALP(LV2),SXX(LV2),SYY(LV2)
CCC   WRITE(9,1030) N,TIME,TXX(LV1),TXX(LV2),TXX(LV3),TXX(LV4),TXX(LV5)
C     WRITE(9,1030) N,TIME,TXX(LV1),TXX(LV2),TXX(LV3),TXX(LV4),TXX(LV5)
C     WRITE(8,1030) N,TIME,P(LV1),EVV(LV1),ALP(LV1),XD(LV1),EJ(LV1)
      WRITE(9,1030) N,TIME,TXX(LV1),TXX(LV2),TXX(LV3),TXX(LV4),TXX(LV5)
 1031 FORMAT(I5,11E11.4)
C
C---TAPE 8 FOR N,TIME,DT
C
      WRITE(8,811) N,TIME,DT
C 811 FORMAT(I5,2E10.3)
C
      IF(N.NE.NNN) GO TO 951
      WRITE(3,2224)
 2224 FORMAT(3X,'J',3X,'K',2X,'LVARM',11X,'X',10X,'XD',9X,'TXX',
     *9X,'TYY',12X,'P',9X,'TXY',9X,'SXX',9X,'SYY',8X,'ALPA',//)
      NNN=NNN+NN
      IF(N.LT.145) GO TO 951
      DO 950 K=1,KCHEK
      DO 920 J=1,JMAX
C
      LVARM=LVAR(K,J)
      IF(LVARM.LE.0) GO TO 920
      IF(M(LVARM).LE.0.AND.J.EQ.1) GO TO 920
      WRITE(3,1040) J ,K,LVARM ,X(LVARM),XD(LVARM),TXX(LVARM)
     *,TYY(LVARM),P(LVARM),TXY(LVARM),SXX(LVARM),SYY(LVARM),ALP(LVARM)
C
```

```
C---DISK 9 FOR N,J,K,X,Y,XD,YD,P,E
C   DISK10 FOR N,J,K,EXX,EYY,EXY,EZZ,ALPA,EVV
C   DISK11 FOR N,J,K,TXX,TYY,TXY,TZZ,SXX,SYY,SZZ
C
C      WRITE(9,911) N,J,K,X(LVARM),Y(LVARM),XD(LVARM),YD(LVARM)
C     +,P(LVARM),E(LVARM)
C 911 FORMAT(3I5,6E10.3)
C
C      WRITE(10,911) N,J,K,EXX(LVARM),EYY(LVARM),EXY(LVARM),
C     +EZZ(LVARM),ALPA(LVARM),EVV(LVARM)
C
      WRITE(11,1111) N,J,K,X(LVARM),Y(LVARM),TXX(LVARM),TYY(LVARM),
     +TZZ(LVARM),TXY(LVARM)
 1111 FORMAT(3I5,6E10.3)
CCC    WRITE(10,1111) N,J,K,X(LVARM),Y(LVARM),XD(LVARM),P(LVARM),
CCC   +TXY(LVARM),TYY(LVARM)
  920 CONTINUE
  990 CONTINUE
  991 CONTINUE
C
      DTB=DT
      DT=DMIN1(0.9*DTW,DMAX1(1.2*DT,0.035*DTW))
      DTB=0.5*(DT+DTN)
      IF(DT.GT.1.E-12) GO TO 100
C
      WRITE(3,1020)
 1020 FORMAT(1X,'STABILITY')
 1030 FORMAT(I5,7E10.3)
 1040 FORMAT(3I5,2X,10E12.5)
C
      STOP
      END
C
C
      SUBROUTINE LAYOUT(JSIZE,JXX,KXX,XL,YL,MM,LVAR)
      IMPLICIT REAL*8(A-H,O-Z)
C
      COMMON/T/X(3000),Y(3000),XD(3000),YD(3000),M(3000),A(3000)
     +,Z(3000),D(3000),SXX(3000),SYY(3000),SZZ(3000),TXY(3000)
     +,TXX(3000),TYY(3000),TZZ(3000),P(3000),E(3000),YY(3000),
     +EVV(3000),EXX(3000),EYY(3000),EZZ(3000),EXY(3000),ALP(3000),
     +IH(3000)
      COMMON/EQS/EQSTC(6),EQSTD(6),EQSTS(6),RHO(6),YC(6),UMU(6)
     +,CLIN(6),CQSQ(6),TRIQ(6),SP(6),EQSTG(6)
      COMMON/GEN/UZERO,DT,DTN,DTW,IJBOND,JMAX,JMIN,KMAX,KMIN,KCHEK
      COMMON/IND/ NFR(10)
      COMMON/FSB/ TSB(10)
      COMMON/POR/ ALP(3000),SXXS(3000),SYYS(3000),SZZS(3000),TXYS(3000)
     +,TYYS(3000),TZZS(3000),TXYS(3000),PS(3000),EVVS(3000),EXXS(3000)
     +,EYYS(3000),EZZS(3000),EXYS(3000),EJ(3000),ALPO(6),IPOR(6),CTCS(6)
      DIMENSION XI(KXX,JXX),YL(KXX,JXX),MM(KXX,JXX),LVAR(KXX,JXX)
     +,XA(4),YA(4)
C
C---
C
      DO 102 J=1,3000
      X(J)=0.
      Y(J)=0.
      XD(J)=0.
      YD(J)=0.
      M(J)=0.
      A(J)=0.
      Z(J)=0.
      D(J)=0.
      SXX(J)=0.
      SYY(J)=0.
      SZZ(J)=0.
      TXY(J)=0.
      TXX(J)=0.
      TYY(J)=0.
      TZZ(J)=0.
```

```
      P(J)=0.
      E(J)=0.
      YY(J)=0.
C
      ALP(J)=0.
      SXXS(J)=0.
      SYYS(J)=0.
      SZZS(J)=0.
      TXXS(J)=0.
      TYYS(J)=0.
      TZZS(J)=0.
      TXYS(J)=0.
      PS(J)=0.
      EVVS(J)=0.
      EXXS(J)=0.
      EYYS(J)=0.
      EZZS(J)=0.
      EXYS(J)=0.
      EJ(J)=0.
C
  10  CONTINUE
C
      JK=JXX*KXX
C
      DO 104 I=1,KXX
      DO 104 J=1,JXX
      XL(I,J)=-999.
      YL(I,J)=-999.
      MM(I,J)=0
  104 LVAR(I,J)=0
C
      KMAX=KXX
      JMAX=JXX
C
      READ(1,1010) IJBUND,NBLOCK,NMTRS,IVTYPE,KCHEK
      WRITE(3,2121) IJBUND,NBLOCK,NMTRS,IVTYPE,KCHEK
 2121 FORMAT(1X,'IJBUND=',I2,3X,'NBLOCK=',I2,3X,'NMTRS=',I2,3X,
     *'IVTYPE=',I2,3X,'KCHEK=',I2,//)
C
      DO 105 I=1,NMTRS
      READ(1,1011) EQSTC(I),EQSTD(I),EQSTG(I),EQSTS(I),IPOR(I)
      WRITE(3,2122) EQSTC(I),EQSTD(I),EQSTG(I),EQSTS(I),IPOR(I)
 2122 FORMAT(1X,'EQSTC=',E12.5,3X,'EQSTD=',E12.5,3X,'EQSTG=',E12.5
     *,3X,'EQSTS=',E12.5,3X,'IPOR=',I2,/)
      READ(1,1012) RHO(I),YC(I),UMU(I),SP(I),NFR(I)
      WRITE(3,2123) RHO(I),YC(I),UMU(I),SP(I),NFR(I)
 2123 FORMAT(1X,'DENSITY=',E12.5,3X,'YC=',E12.5,3X,'SHEAR MOD.=',E12.5,
     *3X,'SOUND SPEED=',E12.5,3X,'FRACTURE OPT.=',I2,/)
      READ(1,1104) CQSQ(I),CLIN(I),TRIQ(I)
      WRITE(3,2215) CQSQ(I),CLIN(I),TRIQ(I)
 2215 FORMAT(1X,'CQSQ=',F10.5,3X,'CLIN=',F10.5,3X,'TRIQ=',F10.5,/)
      IF(IPOR(I).EQ.0) GO TO 114
      READ(1,1011) CTCS(I),ALPO(I)
      WRITE(3,3233) CTCS(I),ALPO(I)
 3233 FORMAT(1X,'CTCS=',E10.3,3X,'ALPO=',F10.5,//)
C
  114 IF(NFR(I).EQ.0) GO TO 105
      READ(1,1011) TSR(I)
      WRITE(3,4344) TSR(I)
 4344 FORMAT(1X,'FRACTURE STRESS=',E12.5)
C
  105 CONTINUE
C
C--CELL LAYOUT
C
      DO 250 NB=1,NBLOCK
      READ(1,1030) K1,K2,(XA(I),I=1,4),MAT
      WRITE(3,6580) K1,K2,(XA(I),I=1,4),MAT
      READ(1,1030) J1,J2,(YA(I),I=1,4)
      WRITE(3,6590) J1,J2,(YA(I),I=1,4)
 6580 FORMAT(1X,'K=',3X,2I5,3X,'X=',4E12.5,3X,'MAT=',I3)
 6590 FORMAT(1X,'J=',3X,2I5,3X,'Y=',4E12.5,/)
```

```
C
      DJDK=(J2-J1)*(K2-K1)
C
      DO 210 K=K1,K2
      DO 210 J=J1,J2
      IF(XL(K,J).EQ.-999.)  XL(K,J)=((XA(1)*(J2-J)+XA(4)*(J-J1))*(K2-
     +K)+(XA(2)*(J2-J)+XA(3)*(J-J1))*(K-K1))/DJDK
      IF(YL(K,J).EQ.-999.)  YL(K,J)=((YA(1)*(J2-J)+YA(4)*(J-J1))*(K2-
     +K)+(YA(2)*(J2-J)+YA(3)*(J-J1))*(K-K1))/DJDK
C
      IF(K.GT.K1 .AND. J.GT.J1)  MM(K,J)=MAT
C
  210 CONTINUE
  250 CONTINUE
C
      LVARM=1
      JM=
C
      DO 300 K=1,KMAX
      DO 280 J=1,JMAX
C
      IF(J.LE.1)  GO TO 261
      IF(LVAR(K,J-1).GT.0)  LVAR(K,J)=-1
  261 IF(XL(K,J).EQ.-999..OR.YL(K,J).EQ.-999.)  GO TO 280
C
      KM=K
      JM=MAXO(JM,J)
      LVAR(K,J)=LVARM
      X(LVARM)=XL(K,J)
      Y(LVARM)=YL(K,J)
      M(LVARM)=MM(K,J)
      IH(LVARM)=2
      MAT=MM(K,J)
      IF(MAT.EQ.0)  GO TO 260
C
      A124=0.5*(XL(K,J-1)*(YL(K,J)-YL(K-1,J))-XL(K,J)*(YL(K,J-1)
     *-YL(K-1,J))+XL(K-1,J)*(YL(K,J-1)-YL(K,J)))
      A234=0.5*(XL(K,J-1)*(YL(K-1,J)-YL(K-1,J-1))+XL(K-1,J)*
     *(YL(K-1,J-1)-YL(K,J-1))+XL(K-1,J-1)*(YL(K,J-1)-YL(K-1,J)))
C
      XZ=0.25*(XL(K,J)+XL(K,J-1)+XL(K-1,J)+XL(K-1,J-1))
      YZ=0.25*(YL(K,J)+YL(K,J-1)+YL(K-1,J)+YL(K-1,J-1))
C
      D(LVARM)=RHO(MAT)
      IF(IPOR(MAT).NE.0)  D(LVARM)=RHO(MAT)*ALPO(MAT)
      IF(IPOR(MAT).NE.0)  ALP(LVARM)=ALPO(MAT)
C
      A(LVARM)=A124+A234
      D(LVARM)=D(LVARM)*A(LVARM)
      IF(YC(MAT).NE.0.)  YY(LVARM)=YC(MAT)
  260 CONTINUE
C
      LVARM=LVARM+1
  280 CONTINUE
  300 CONTINUE
C
      KMAX=KM
      JMAX=JM
C
      WRITE(3,132)  KMAX,JMAX
  132 FORMAT(1X,'KMAX=',I5,5X,'JMAX=',I5,/)
C
C
C--INITIALIZE VEL. IN ONE BLOCK
C
      IF(IVTYPE.EQ.0)  GO TO 450
      READ(1,1032)  JB,JU,KU,UZERO
      WRITE(3,2143)  JB,JU,KU,UZERO
 2143 FORMAT(1X,'JB=',I2,3X,'JU=',I2,3X,'KU=',I2,3X,'UZERO=',E12.5)
C
      AMASS=0.
      BMASS=0.
      SKU=1.
```

```
      BKU1=1.
      UZINT=UZERO
C
      DO 310 J=2,JJ
      IF(MM(KU,J).LE.0 .OR. MM(KU+1,J).LE.0) GO TO 310
      MA=MM(KU,J)
      IF(IPOR(MA).NE.0) BKU=ALPO(MA)
      MB=MM(KU+1,J)
      IF(IPOR(MB).NE.0) BKU1=ALPO(MB)
      AMASS=AMASS+BKU*RHO(MA)*(XL(KU,J)-XL(KU-1,J))
      BMASS=BMASS+BKU1*RHO(MB)*(XL(KU+1,J)-XL(KU,J))
  310 CONTINUE
C
      IF(AMASS+BMASS.GT.0..AND.IVTYPE.EQ.-1) UZINT=UZERO*BMASS/
     &(AMASS+BMASS)
      IF(AMASS+BMASS.GT.0. .AND. IVTYPE.EQ.1) UZINT=UZERO*AMASS/
     &(AMASS+BMASS)
C
      DO 325 K=1,KMAX
      DO 325 J=1,JMAX
      IF(LVAR(K,J).LE.0 ) GO TO 320
      LM=LVAR(K,J)
C
      IF(K.GT.KU.AND.IVTYPE.EQ.-1) XD(LM)=UZERO
      IF(K.LT.KU.AND.IVTYPE.EQ.1) XD(LM)=UZERO
      IF(J.LE.JU.AND.K.EQ.KU.AND.J.GE.JB) XD(LM)=UZINT
C
  320 CONTINUE
  325 CONTINUE
C
      IF(KCHEK.NE.0) GO TO 450
      KCHEK=KMAX
      IF(IVTYPE.EQ.1) KCHEK=KU+3
C
  450 CONTINUE
C
      WRITE(3,1250)
      ZERO=0.
C
      DO 470 K=1,KMAX
      DO 460 J=1,JMAX
      LM=LVAR(K,J)
      IF(LM.LE.0) GO TO 460
      IF(MM(K,J).GT.0) GO TO 455
      WRITE(3,1280) J,K,MM(K,J),LM,X(LM),Y(LM),ZERO,ZERO,ZERO,ZERO
     &,XD(LM),YD(LM),ZERO
      GO TO 460
  455 MAT=MM(K,J)
      YYY=0.
      IF(YC(MAT).NE.0) YYY=YY(LM)
      WRITE(3,1280) J,K,MAT,LM,X(LM),Y(LM),A(LM),D(LM),Z(LM),YYY,XD(LM)
     &,YD(LM),E(LM)
  460 CONTINUE
  470 CONTINUE
C
 1010 FORMAT(5I5)
 1100 FORMAT(3F10.3)
 1011 FORMAT(4E10.3,I5)
 1012 FORMAT(4E10.3,I5)
 1030 FORMAT(2I5,4E10.3,I5)
 1032 FORMAT(3I5,E10.3)
 1250 FORMAT(1H1,4X,'J',4X,'K',4X,'M',' LVAR',11X,'X',11X,
     * 1HY,11X,1HA,11X,1HD,11X,1HZ,7X,5HYIELD,10X,2HXD,10X,2HYD,11X,
     * 1HE)
 1280 FORMAT(4I5,9F12.6,4(1X,E12.6))
C
      RETURN
      END
C
C
      SUBROUTINE SWEEP(JSIZE,JXX,KXX,XL,YL,MM,LVAR)
      IMPLICIT REAL*8(A-H,O-Z)
```

```
C       COMMON/T/X(3000),Y(3000),XD(3000),YD(3000),M(3000),A(3000)
     +,Z(3000),D(3000),SXX(3000),SYY(3000),SZZ(3000),TXY(3000)
     +,TXX(3000),TYY(3000),TZZ(3000),P(3000),E(3000),YY(3000),
     +EVV(3000),EXX(3000),EYY(3000),EZZ(3000),EXY(3000),ALP(3000),
     +IH(3000)
       COMMON/EQS/EQSTC(6),EQSTD(6),EQSTS(6),RHO(6),YC(6),UMU(6)
     +,CLIN(6),CQSQ(6),TBIQ(6),SP(6),EQSTG(6)
       COMMON/GEN/UZERO,DT,DTH,DTW,IJBUND,JMAX,JMIN,KMAX,KMIN,KCHEK
       COMMON/IND/ NFB(10)
       COMMON/FSB/ TSR(10)
       COMMON/POR/ ALP(3000),SXXS(3000),SYYS(3000),SZZS(3000),TXXS(3000)
     +,TXYS(3000),TZZS(3000),TXYS(3000),PS(3000),EVVS(3000),EXXS(3000)
     +,EYYS(3000),EZZS(3000),EXYS(3000),EJ(3000),ALPO(6),IPOR(6),CTCS(6)
       DIMENSION XI(KXX,JXX),YL(KXX,JXX),MM(KXX,JXX),LVAR(KXX,JXX)
       DIMENSION XTEMP(100),YTEMP(100),XDTEMP(100),YDTEMP(100)

C      DO 123 I=1,100
       XTEMP(I)=0.
       YTEMP(I)=0.
       XDTEMP(I)=0.
  123  YDTEMP(I)=0.
C
       DTS_M=1.
C
       DO 950 K=1,KMAX
       DO 920 J=1,JMAX
C
       LVARM=LVAR(K,J)
       IF(LVARM.LE.0) GO TO 780
C
       DM=0.
       TXXM=0.
       TYYM=0.
       TZZM=0.
       TXYM=0.
       SXXM=0.
       SYYM=0.
       SZZM=0.
       EM=0.
       PM=0.
       Q=0.
       SPSQ=0.
C
C---MOMENTUM
C
       XDMM=XD(LVARM)
       YDMM=YD(LVARM)
       FX=0.
       FY=0.
       XMOM=0.
       AMASS=0.
       L3=LVARM
C
C--FIND THE COORD. OF CELLS AROUND POINT (K,J)
C
       DO 360 I=1,4
C
C      WRITE(3,1456) K,J,I
C1456 FORMAT(1X,'--------',3I5)
C
       DMASS=0.
       GO TO (230,240,250,260),I
C
C--I=1, UPPER RIGHT HAND QUADRANT
C
  230 IF(K.EQ.KMAX.OR.J.EQ.JMAX) GO TO 360
       IF(MM(K+1,J+1).LE.0) GO TO 360
C
       L1=LVAR(K+1,J+1)
       L2=LVAR(K,J+1)
       L4=LVAR(K+1,J)
```

```
      LB=L1
      MAT=MM(K+1,J+1)
      GO TO 270
C
C--I=2,UPPER LEFT
C
  240 IF(K.EQ.1.OR.J.EQ.JMAX) GO TO 360
      IF(MM(K,J+1).LE.0) GO TO 360
C
      L1=LVAR(K-1,J+1)
      L2=LVAR(K-1,J)
      L4=LVAR(K,J+1)
      LB=L4
      MAT=MM(K,J+1)
      GO TO 270
C
C--I=3, LOWER LEFT
C
  250 IF(K.EQ.1.OR.J.EQ.1) GO TO 360
      IF(MM(K,J).LE.0) GO TO 360
C
      L1=LVAR(K-1,J-1)
      L2=LVAR(K,J-1)
      L4=LVAR(K-1,J)
      LB=L3
      MAT=MM(K,J)
      GO TO 270
C
C---I=4, LOWER RIGHT
C
  260 IF(K.EQ.KMAX.OR.J.EQ.1) GO TO 360
      IF(MM(K+1,J).LE.0) GO TO 360
C
      L1=LVAR(K+1,J-1)
      L2=LVAR(K+1,J)
      L4=LVAR(K,J-1)
      LB=L2
      MAT=MM(K+1,J)
      GO TO 270
C
  270 CONTINUE
C
  300 X02=0.5*(X(L1)+X(L2)+X(L3)+X(L4))
      Y02=0.5*(Y(L1)+Y(L2)+Y(L3)+Y(L4))
C
  305 A0=(X02-X(L3))*(Y(L2)-Y(L4))+X(L2)*(Y(L3)+Y(L4)-Y02)+X(L4)
     +*(Y02-Y(L2)-Y(L3))
      A3=X(L4)*(Y(L2)-Y(L3))-X(L3)*(Y(L2)-Y(L4))+X(L2)*(Y(L3)-Y(L4))
C
      AXY=(A0+A3)/8.
      AXX=(Y(L2)-Y(L4))/2.
      AYY=(X(L4)-X(L2))/2.
      TZZAXY=0.
C
      IF(DMASS.NE.0.) GO TO 330
      DMASS=D(LB)*AXY
      GO TO 330
C
  320 QXX=0.
      QYY=0.
      QXY=0.
C
C--STRAINS ARE POSITIVE IN TENSION
C
      IF(TRIQ(MAT).EQ.0. .OR.A3.LE.0.1*AXY) GO TO 340
C
      EDXX=((XD(L2)-XD(L3))*(Y(L2)-Y(L4))-(XD(L2)-XD(L4))*(Y(L2)-
     + Y(L3)))/A3
      EDYY=-((YD(L2)-YD(L3))*(X(L2)-X(L4))-(YD(L2)-YD(L4))*(X(L2)-
     + X(L3)))/A3
      EDXY=(-(XD(L2)-XD(L3))*(X(L2)-X(L4))+(XD(L2)-XD(L4))*(X(L2)-
     1 X(L3))+(YD(L2)-YD(L3))*(Y(L2)-Y(L4))-(YD(L2)-YD(L4))*(Y(L2)-
     2 Y(L3)))/A3
```

```
C
C--TRIANGLE Q STRESSES ARE POSITIVE IN TENSION
C
       COEF=DSQRT(A3)*SP(MAT)*D(LM)*TRIQ(MAT)
      QXX=COEF*(2.*EDXX-EDYY)
      QYY=COEF*(2.*EDYY-EDXX)
      QXY=3.*COEF*EDXY
C
  340 FX=FX+(TXX(LM)+QXX)*AXX+(TXY(LM)+QXY)*AYY
      FY=FY+(TXY(LM)+QXY)*AXX+(TYY(LM)+QYY)*AYY-TZZAXY
C
      AMASS=AMASS+DMASS
C
C     WRITE(3,1978) L1,L2,L3,L4,MAT,A0,A3,AXX,AYY
C     WRITE(3,1798) QXX,QYY,QXY,FX,FY,AMASS
C1978 FORMAT(5I5,4E12.4)
C1798 FORMAT(6E12.4)
C
C
  360 CONTINUE
C
C--POS. AND VEL.
C
      LM=LVAB(K,J)
      IJBABS=IABS(IJBUND)
C
      IF(J.EQ.JMAX.AND.(IJBABS.EQ.1.OR.IJBABS.EQ.5)) GO TO 347
      IF(J.EQ.1.AND.IJBUND.NE.-3) GO TO 347
  345 YDNH=YD(LM)+DTN*FY/AMASS
  347 YNW=Y(LM)+YDNH*DT
C
      IF(K.EQ.1.AND.(IJBABS.EQ.4.OR.IJBABS.EQ.5.OR.
     * IJBABS.EQ.6)) GO TO 357
      IF(K.EQ.KMAX.AND.IJBABS.EQ.4) GO TO 357
C
  356 XDNH=XD(LM)+DTN*FX/AMASS
C
  357 XNW=X(LM)+XDNH*DT
C
      IF(MS(K,J).EQ.0) GO TO 750
C
C--NEW AREA AND VOL. FOR CELL K,J
C
      A124=XTEMP(J-1)*(YNW-YTEMP(J))-XNW*(YTEMP(J-1)-YTEMP(J))+
     1 XTEMP(J)*(YTEMP(J-1)-YNW)
      LM=LVAB(K,J)
      LMN=LVAB(K-1,J-1)
      LKM=LVAB(K,J-1)
      LMJ=LVAB(K-1,J)
C
      A234=XTEMP(J-1)*(YTEMP(J)-YKMJM)+XTEMP(J)*(YKMJM-YTEMP(J-1))+
     1   XKMJM*(YTEMP(J-1)-YTEMP(J))
C
  420 AW=0.5*(A124+A234)
      IF(AW.GT.0.) GO TO 425
      WRITE(3,1010) K,J
 1010 FORMAT('WWWWWWWWWWWWWWWWWWWWRRRRRRRRRRR',2I5)
  425 CONTINUE
      DW=Z(LM)/AW
C
C     WRITE(3,1567) K,J,A124,A234,AW,DW
C1567 FORMAT(1X,2I5,4E15.4)


C
C--COMPUTE STRAINS
C
      DTA=DT/(AW+A(LM))
      XM13=(X(LM)+XNW)/2.-XHMM
      XM42=(XTEMP(J-1)+X(LKM)-XTEMP(J)-X(LMJ))/2.
      YM13=(Y(LM)+YNW)/2.-YHMM
      YM42=(YTEMP(J-1)+Y(LKM)-YTEMP(J)-Y(LMJ))/2.
      XDM13=XDNH-XD(LMN)
      XDM42=XDTEMP(J-1)-XDTEMP(J)
```

```
      YDH13=YDHH-YD(LMM)
      YDH42=YDTEMP(J-1)-YDTEMP(J)
C
C--DEFINE COORD. OF CELL
C
      X1=0.5*(X(LM)+XMM)
      X2=0.5*(XTEMP(J)+X(LMJ))
      X3=XHMM
      X4=0.5*(XTEMP(J-1)+X(LKM))
C
      Y1=0.5*(Y(LM)+YMM)
      Y2=0.5*(YTEMP(J)+Y(LMJ))
      Y3=YHMM
      Y4=0.5*(YTEMP(J-1)+Y(LKM))
C
C--SQUARED OF VECTORS
C
      XMAG43=(X4-X3)**2+(Y4-Y3)**2
      XMAG41=(X4-X1)**2+(Y4-Y1)**2
      XMAG12=(X1-X2)**2+(Y1-Y2)**2
      XMAG23=(X2-X3)**2+(Y2-Y3)**2
C
C--DOT PROD
C
      D432=-((X4-X3)*(X3-X2)+(Y4-Y3)*(Y3-Y2))
      D321=-((X3-X2)*(X2-X1)+(Y3-Y2)*(Y2-Y1))
      D143=-((X1-X4)*(X4-X3)+(Y1-Y4)*(Y4-Y3))
      D214=-((X2-X1)*(X1-X4)+(Y2-Y1)*(Y1-Y4))
C
C-- CHECK TO SEE IF PROJECTION LIES INSIDE CELL
C
      IF( D432.LE.0.) D432=0.
      IF( D321.LE.0.) D321=0.
      IF( D214.LE.0.) D214=0.
      IF( D143.LE.0.) D143=0.
C
      D432=D432**2
      D321=D321**2
      D214=D214**2
      D143=D143**2
C
C--FIND THE MINIMUM DISTANCE
C
      DELX=DMIN1(XMAG43-D432/XMAG23,
     1           XMAG23-D432/XMAG43,
     2           XMAG23-D321/XMAG12,
     3           XMAG12-D321/XMAG23,
     4           XMAG12-D214/XMAG41,
     5           XMAG41-D214/XMAG12,
     6           XMAG41-D143/XMAG43,
     7           XMAG43-D143/XMAG41 )
C
      EVOL=2.*(D(LM)-DW)/(D(LM)+DW)
      EXXH=DTA*(XDH42*YH13-YH42*XDH13)
      EYYH=-DTA*(YDH42*XH13-XH42*YDH13)
      EXYH=0.5*DTA*(YDH42*YH13-YH42*YDH13-XDH42*XH13+XH42*XDH13)
      EZZH=EVOL-EXXH-EYYH
      ALFA=0.5*DTA*(-YDH42*YH13+YH42*YDH13-XDH42*XH13+XH42*XDH13)
  430 MAT=MM(K,J)
C
C     WRITE(3,3562) J,K,DELX,EVOL,EXXH,EYYH,EZZH,EXYH,ALFA
C3562 FORMAT(2I5,7E12.4)
C
C
C--VISCOSITY
C
      SPR=1.
      IF(IPOR(MAT).NE.0) SPR=1.+(1.-ALP(LM))/(1.-ALPO(MAT))*(
     +CICS(MAT)-1.)
C
      DELD=DW-D(LM)
      IF(DELD.GT.C.)
```

```
     +Q=DELD/DT*(SPR*SP(MAT)*CLIN(MAT)*DSQRT(AW)+CQSQ(MAT)
     +*AW*DELD/DW/DT)
C      IF(DELD.LT.0.AND.IPOR(MAT).NE.0)
C     +Q=DELD/DT*(SPR*SP(MAT)*CLIN(MAT)*DSQRT(AW)+CQSQ(MAT)
C     +*AW*DELD/DW/DT)
C
C--ESTIMATE INTERNAL ENERGY
C
      DELZ=(SXX(LM)*EXXH+SYY(LM)*EYYH+SZZ(LM)*EZZH+2.*TXY(LM)*EXYH)/DW
      EW=E(LM)+DELZ-(P(LM)+Q)*(1./DW-1./D(LM))
      EAVG=EVOL/3.
      BETA=2.*TXY(LM)*ALFA
C
      IF(IPOR(MAT).EQ.0) GO TO 601
      CALL POREL(DW,EVOL,EXXH,EYYH,EZZH,EXYH,SXXW,SYYW,SZZW,TXYW,PW,
      EW,BETA,ALFA,LM,MAT,K,J)
      GO TO 630
C
C
C--ELASTIC MATERIAL
C
  601 CALL EOST (EW,DW,PW,MAT)
C
C
      SXXW=SXX(LM)+2.*UMU(MAT)*(EXXH-EAVG)+BETA
      SYYW=SYY(LM)+2.*UMU(MAT)*(EYYH-EAVG)-BETA
      SZZW=SZZ(LM)+2.*UMU(MAT)*(EZZH-EAVG)
C
      TXYW=TXY(LM)+2.*UMU(MAT)*EXYH+(SYY(LM)-SXX(LM))*ALFA
C
C---Y-M MODEL
C
      IF(YC(MAT).LE.0.) GO TO 600
      SJ2=SXXW**2+SYYW**2+SZZW**2+2.*TXYW**2
      YYY=0.666667*YY(LM)**2
      IF(SJ2.LE.YYY) GO TO 600
C
      CY=DSQRT(YYY/SJ2)
      SXXW=CY*SXXW
      SYYW=CY*SYYW
      SZZW=CY*SZZW
      TXYW=CY*TXYW
C
C--ADJUST INTERNAL ENERGY
C
  600 EW=E(LM)+0.5*((SXX(LM)+SXXW)*EXXH+(SYY(LM)+SYYW)*EYYH+(SZZ(LM)+
     1 SZZW)*EZZH+2.*(TXY(LM)+TXYW)*EXYH)/DW-((P(LM)+PW)/2.+Q)*(1./
     2DW-1./D(LM))
C
C-- COMPUTE TOTAL STRESS
C
  620 TXXW=SXXW-PW-Q
      TYYW=SYYW-PW-Q
      TZZW=SZZW-PW-Q
C
C---SEPARATION OF IMPACT PLANE
C
      IF(NPR(MAT).NE.5.AND.NPR(MAT).NE.6) GO TO 690
      IF(NPR(MAT).EQ.6) GO TO 650
      IF(TXXW.LE.TSR(MAT)) GO TO 690
C
      P1=TXXW*EQSTC(MAT)/(EQSTC(MAT)+1.3333*UMU(MAT))
      DSX=1.3333*TXXW*UMU(MAT)/(EQSTC(MAT)+1.3333*UMU(MAT))
C
      TXXW=TXXW-DSX-P1
      TYYW=TYYW-P1+DSX/2.
      TZZW=TZZW-P1+DSX/2.
C
      PW=-(TXXW+TYYW+TZZW)/3.
      TXYW=0.
      GO TO 680
```

```
C
  650 IF(TYYW.LE.TSR(MAT)) GO TO 690
C
      P1=TYYW*EQSTC(MAT)/(EQSTC(MAT)+1.3333*UMU(MAT))
      DSY=1.3333*TYYW*UMU(MAT)/(EQSTC(MAT)+1.3333*UMU(MAT))
C
      TXXW=TXXW-P1+DSY/2.
      TYYW=TYYW-P1-DSY
      TZZW=TZZW-P1+DSY/2.
C
      PW=-(TXXW+TYYW+TZZW)/3.
      TXYW=0.
C
  680 IF(IH(LM).EQ.1) GO TO 690
      IH(LM)=1
C
      WRITE(3,1680) K,J
 1680 FORMAT(1X,'SEPARATION AT CELL K,J =',2I4)
C
C--COMPUTE SOUND SPEED AND TIM.
C
  690 EMOD=0.
      SPSQ=SP(MAT)**2
      IF(IPCR(MAT).NE.0) SPSQ=SPSQ*SPR*SPR
      IF(DABS(DW-D(LM)).LT.1.E-8) GO TO 700
      EMOD=PW/(DW/RHO(MAT)-1.)+2.*Q*DW/(DW-D(LM))+1.33*UMU(MAT)
      SPSQ=DMAX1(EMOD/D(LM), .3*SPSQ)
C
  700 DTSQ=DELX/SPSQ
      IF(DTSQ.GE.DTSQM) GO TO 750
C
      KT=K
      JT=J
      DELXT=DELX
      DTSQT=DTSQ
      SPSQT=SPSQ
      DTSQM=DTSQ
C
  750 CONTINUE
  760 CONTINUE
C
      IF(K.EQ.1) GO TO 790
      IF(J.EQ.1) GO TO 785
      LMN=LVAR(K-1,J-1)
      IF(LMN.LE.0) GO TO 785
      X(LMN)=XKMJM
      Y(LMN)=YKMJM
C
  785 CONTINUE
      LMJ=LVAR(K-1,J)
      IF(LMJ.LE.0) GO TO 790
      XMMM=(X(LMJ)+XTEMP(J))/2.
      YMMM=(Y(LMJ)+YTEMP(J))/2.
      XKMJM=XTEMP(J)
      YKMJM=YTEMP(J)
      XD(LMJ)=XDTEMP(J)
      YD(LMJ)=YDTEMP(J)
C
  790 IF(LVARM.LE.0) GO TO 920
      XTEMP(J)=XNW
      YTEMP(J)=YNW
      XDTEMP(J)=XDNW
      YDTEMP(J)=YDNW
      IF(MM(K,J).EQ.0) GO TO 800
C
  795 LM=LVARM
      D(LM)=DW
      E(LM)=EW
      SXX(LM)=SXXW
      SYY(LM)=SYYW
      SZZ(LM)=SZZW
      TXY(LM)=TXYW
      TXX(LM)=TXXW
```

```
      TYY(LM)=TYYM
      TZZ(LM)=TZZM
      P(LM)=PM
      EVV(LM)=EVV(LM)+EVOL
      EXX(LM)=EXX(LM)+EXXH
      EYY(LM)=EYY(LM)+EYYH
      EZZ(LM)=EZZ(LM)+EZZH
      EXY(LM)=EXY(LM)+EXYH
      ALP(LM)=ALP(LM)+ALPA
C
  800 CONTINUE
  920 CONTINUE
C
      IF(K.EQ.1) GO TO 940
      LMJ=LVAR(K-1,JMAX)
      IF(LMJ.LE.0) GO TO 940
      X(LMJ)=XKMJM
      Y(LMJ)=YKMJM
C
  940 KK=K
      IF(K.LT.KCHEK.OR.K.EQ.KMAX) GO TO 950
C
      DO 945 J=1,JMAX
      LMJ=LVAR(K-1,J)
      IF(LMJ.LE.0) GO TO 945
      IF(DABS(XD(LMJ)).GT..1E-3.OR.DABS(YD(LMJ)).GT..1E-3) GO TO 948
  945 CONTINUE
      GO TO 960
  948 KCHEK=MIN0(K+1,KMAX)
      GO TO 960
  950 CONTINUE
  960 CONTINUE
C
      DO 980 J=1,JMAX
      LMJ=LVAR(KK,J)
      IF(LMJ.LE.0) GO TO 980
      X(LMJ)=XTEMP(J)
      Y(LMJ)=YTEMP(J)
      XD(LMJ)=XDTEMP(J)
      YD(LMJ)=YDTEMP(J)
  980 CONTINUE
C
      DTM=DSQRT(DTSJM)*(1.-3.*TRIQ(1))
C
      RETURN
      END
C
C
      SUBROUTINE EQST(Z,D,P,M)
      IMPLICIT REAL*8(A-H,O-Z)
C
      COMMON/E_S/EQSTC(6),EQSTD(6),EQSTS(6),RHO(6),YC(6),UMU(6)
     +,CLIN(6),CQSQ(6),TRIQ(6),SP(6),EQSTG(6)
      EMU=D/RHO(M)-1.
      PH=EMU*(EQSTC(M)+EMU*(EQSTD(M)+EMU*EQSTS(M)))
      P=PH*(1.-0.5*EQSTG(M)*(1.-RHO(M)/D))+EQSTG(M)*RHO(M)*E
      RETURN
      END
C
C
      SUBROUTINE POREL(DM,EVOL,EXXH,EYYH,EZZH,EXYH,SXXM,SYYM,
     +SZZM,TXYM,PM,EM,BETA,ALFA,LM,MAT,K,J)
      IMPLICIT REAL*8(A-H,O-Z)
      COMMON/T/X(3000),Y(3000),XD(3000),YD(3000),M(3000),A(3000)
     +,Z(3000),D(3000),SXX(3000),SYY(3000),SZZ(3000),TXY(3000)
     +,TXX(3000),TYY(3000),TZZ(3000),P(3000),E(3000),YY(3000),
     +EVV(3000),EXX(3000),EYY(3000),EZZ(3000),EXY(3000),ALP(3000),
     +IH(3000)
      COMMON/EQS/EQSTC(6),EQSTD(6),EQSTS(6),RHO(6),YC(6),UMU(6)
     +,CLIN(6),CQSQ(6),TRIQ(6),SP(6),EQSTG(6)
      COMMON/POR/ ALP(3000),SXXS(3000),SYYS(3000),SZZS(3000),TXXS(3000)
     +,TYYS(3000),TZZS(3000),TXYS(3000),PS(3000),EVVS(3000),EXXS(3000)
     +,EYYS(3000),EZZS(3000),EXYS(3000),EJ(3000),ALPO(6),IPOR(6),CTCS(6)
```

```
C
C----ALPQ, ALPA AT PREVIOUS TIME PTO, PRESSURE AT PREVIOUS TIME
C     ALPP,PTP, ARE VARIABLES FOR ITERATION PROCESS
C
      ALPQ=ALP(LM)
C     WRITE(3,123) K,J,LM,ALP(LM),P(LM)
C 123 FORMAT(1X,'BEFORE',3I5,5X,2E12.5)
C 124 FORMAT(1X,'AFTER',3I5,5X,5E12.5)
      ALPP=ALPQ
      PTO=P(LM)
      PTP=PTO
      HH=1.+(1.-ALPQ)/(1.-ALPO(MAT))*(C1CS(MAT)-1.)
      II=1
C
   10 BMOS=DW/ALPP
      CALL EQST(EW,BMOS,PSS,MAT)
C
      PTT=ALPP*PSS
      IF(DABS(PTP-PTT).LE.0.1) GO TO 100
C
C---THE PROCEDURE TO FIND NEW PTP
C
      ANU=BMOS/BMC(MAT)
C
      DAPP=(1./HH/HH-1.)/EQSTC(MAT)
      DAPT=-1./(EQSTC(MAT)+EQSTD(MAT)*(ANU-1.)*(ANU+1.))
C
      PTP=(PTP*DAPP-PTT*DAPT)/(DAPP-DAPT)
      ALPP=ALPQ+(PTP-PTO)/EQSTC(MAT)*(1./HH/HH-1.)
C     WRITE(3,1000) II,LM,BMOS,ALPQ,ALPP,PTT,PTP,HH
C1000 FORMAT(2I5,6E12.5)
      II=II+1
      IF(II.GT.20) CALL EXIT
C
      GO TO 10
  100 CONTINUE
C
C---NEGATIVE PRESURE AT UNDISTURBED CELL IS FORCED TO GO
C   BACK TO ORIGINAL STATE
C
CCC   IF(ALPP.LT.ALPO(MAT)) ALPP=ALPO(MAT)
C
C---NEW ALPA AND PRESSURE WERE DECIDED. NOW GOING FOR DEVIATORIC
C   STRESS
C
      DALP=ALPP-ALPQ
      EAVG=EVOL/3.
      ALVT=1.+DALP/EVOL/ALPP
      IF(ALVT.LE.0.) GO TO 249
      IF(ALVT.GE.1.) ALVT=1.
      GO TO 247
  249 ALVT=0.
  247 ETXX=EXXH-EAVG
      ETYY=EYYH-EAVG
      ETZZ=EZZH-EAVG
C
      ESXX=ALVT*ETXX
      ESYY=ALVT*ETYY
      ESZZ=ALVT*ETZZ
      ESXY=ALVT*EXYH
C
      DSXX=2.*UMU(MAT)*ESXX+BETA
      DSYY=2.*UMU(MAT)*ESYY-BETA
      DSZZ=2.*UMU(MAT)*ESZZ
      DSXY=2.*UMU(MAT)*ESXY+(SYYS(LM)-SXXS(LM))*ALPA
C
      SXXS(LM)=SXXS(LM)+DSXX
      SYYS(LM)=SYYS(LM)+DSYY
      SZZS(LM)=SZZS(LM)+DSZZ
      TXYS(LM)=TXYS(LM)+DSXY
C
      SXXW=ALPP*SXXS(LM)*1.0
      SYYW=ALPP*SYYS(LM)*1.0
```

```
      SZZW=ALPP*SZZS(LM)*1.0
      TXYW=ALPP*TXYS(LM)*1.0
C     WRITE(3,1457) SXXW,SYYW,SZZW,ALVT
C1457 FORMAT(1X,'DEV',4E15.5)
C
C    IN      OUT
C   ALPP                ;RESULT FROM ELASTIC
C ALPO(MAT)             ;INITIAL POROSITY
C EJ(LM)                ;3J2**.5 AT PREVIOUS TIME FOR STARTING POINT
C ALPQ                  ; PREVIOUS ALPA FOR STARTING POINT
C DW                    ; CURRENT TOTAL DENSITY
C PTP                   ; RESULT FROM ELASTIC
C RHO(MAT)              ; INITIAL SOLID DENSITY
C
      CALL ELIPT(ALPP,ALPO(MAT),EJ(LM),ALPQ,DW,PTP,P(LM),RHO(MAT),
     +EQSTC(MAT),EQSTD(MAT),SXXW,SYYW,SZZW,TXYW,K,J)
C
      PW=PTP
      ALP(LM)=ALPQ
      PS(LM)=PW/ALPQ
      SXXS(LM)=SXXW/ALPQ
      SYYS(LM)=SYYW/ALPQ
      SZZS(LM)=SZZW/ALPQ
      TXYS(LM)=TXYW/ALPQ
C
  243 RETURN
      END
C
C
      SUBROUTINE ELIPT(ALPO,ALPP,EJP,ALPA1,RHO,PP,PRP,RHOS,AP,BP,SXXW
     +,SYYW,SZZW,TXYW,K,J)
      IMPLICIT REAL*8(A-H,O-Z)
C
C---EJ,ALPA1 AT PREVIOUS STEP FOR STARTING POINT
C
      AAA=1.00
      Y=2.0D06
      BETA= 6.
C---PUT PREVIOUS ALPA FOR CHECKING PLASTIC RANGE
      ALPA=ALPA1
      EJ=EJP
      P=PP
      QC=1.000
      AM=2.D00
      C=.0D00
      CP=.75
      CK=1.00D06
C---CURRENT DEVIATORIC TERM
      SUM=SXXW*SXXW+SYYW*SYYW+SZZW*SZZW+2.*TXYW*TXYW
      EJO=DSQRT(1.5*SUM)
      EJ1=EJO
      II=1
      KK=1
C
C----CARROLL-HOLT'S PRESSURE EQUATION
C
      R1=2.D00/3.D00
C
      GO TO 100
   90 II=2
CCC   IF(PP.GT.PRP ) GO TO 100
C
C----PLASTIC UNLOADING
C
CCC   CALL PLAST(P1,Y1,QO,AM,C,CK,PRP,PP,EJP,EJO,EJ1)
CCC   KK=2
CCC   GO TO 400
C
C---STARTED WITH PREVIOUS ALFA
C
  100 R2=R1*BETA
      R3=AAA-ALFA
```

```
C
      P1=Y/BETA*(1.D00/R3**R2-CP/(AAA-ALPP)**R2)
      DP1=1.*R1*Y/R3**(R2+1.D00)
      DDP1=1.*R1*Y*(R2+1.D00)/R3**(R2+2.D00)
C
C-----PRESSURE-ALFA RELATION
C
      R4=RHO/ALFA/RHOS
      R5=R4-1.D00
C
      IF(II.EQ.1) GO TO 799
      P=ALFA*(AP*R5+BP*R5*R5)
      DP=-AP-BP*(R4*R4-1.)
      DDP=2.D00*BP/ALFA*R4*R4
C
C-----DEVIATORIC TERM AND ALFA
C
  799 Y1=QO*R3**AM*P1
      DY1=QO*(-AM*R3**(AM-1.D00)*P1+R3**AM*DP1)
      DDY1=QO*(AM*(AM-1.D00)*R3**(AM-2.D00)*P1-2.D00*AM*R3**(AM-1.D
     +          00)*DP1 +R3**AM*DDP1)
C
C---A AND B
C
      R6=1.D00-C
      R7=1.D00+C
C
      A=2.D00*P-R6*P1+OK
      DA=2.D00*DP-R6*DP1
      DDA=2.D00*DDP-R6*DDP1
C
      B=R7*P1+OK
C
      IF(II.EQ.1) GCOM=A*A/B/B+EJO*EJO/Y1/Y1-1.
      IF(II.EQ.1.AND.GCOM.GT.0.) GO TO 90
C     WRITE(3,1200) GCOM,A,B,EJO,Y1
C1200 FORMAT(1X,'GCOM',5E15.5)
      IF(II.EQ.1.AND.GCOM.LE.0.) GO TO 300
C
      DB=R7*DP1
      DDB=R7*DDP1
C
C---YIELD FUNCTION
C
      G=A*A/B/B+EJ*EJ/Y1/Y1-1.D00
      GA=2.D00*(A*DA-A*A*DB/B)/(B*B)-EJ*EJ*DY1/Y1/Y1/Y1
      GAA=DA*DA+3.D00*A*A*DB*DB/B/B-4.D00*A*DA*DB/B
      GAA=(GAA+A*DDA-A*A*DDB/B)/B/B
      GAA=2.D00*(GAA+EJ*EJ/Y1/Y1/Y1*(3.D00*DY1*DY1/Y1-DDY1))
C
      GJ=2.D00*EJ/Y1/Y1
      GJJ=2.D00/Y1/Y1
      GAJ=-4.D00*EJ/Y1*DY1/Y1/Y1
C
C---  ELEMENT OF JACOBIAN
C
      AJ11=2.D00*(GJ+(ALFA-ALFO)*GAJ-(EJ-EJO)*GAA)
      AJ12=2.D00*((ALFA-ALFO)*GJJ-GA-(EJ-EJO)*GAJ)
      AJ21=GA
      AJ22=GJ
C
      DET=AJ11*AJ22-AJ12*AJ21
C
C---ANOTHER NONLINEAR EQ. WITH YIELD FUNCTION
C
      F=2.D00*(ALFA-ALFO)*GJ-2.D00*(EJ-EJO)*GA
C
C-----NEW ALFA AND DEV. TERM
C
      ALFAA=ALFA-(AJ22*F-AJ12*G)/DET
      EJ1=EJ-(-AJ21*F+AJ11*G)/DET
```

```
C
C---EJJ FROM YIELD FUNCTION DIRECTLY
C
      EJJ=2.D00*DSQRT(DABS((P1-P)*(P+OK+C*P1)))
      EJJ=EJJ/(P1+OK+C*P1)*Y1
      IF(II.GE.45) WRITE(3,1000)K,J,II,ALPA,RHO,EJ,EJJ,P,P1,F,G
 1000 FORMAT(3I5, 8E12.5)
C
      EBB=1.0D-08
      STOC=DABS((EJ1-EJ)/EJ1)
      STOD=DABS((ALPAA-ALPA)/ALPAA)
      IF(STOC.LE.EBB.AND.STOD.LE.EBB) GO TO 400
C
      EJ=EJ1
      ALPA=ALPAA
      PP=P
      GG=G
      II=II+1
      IF(II.GE.50) WRITE(3,1001)II,RHO,STOC,STOD
      IF(II.GE.50) CALL EXIT
 1001 FORMAT(5X,'NEWTON METHOD DOES NOT CONVERGE',I5,3E15.5)
C
      GO TO 100
C
  400 CONTINUE
      IF(KK.NE.2) PP=P
      EEJJ=EJ1/EJO
      SXXW=SXXW*EEJJ
      SYYW=SYYW*EEJJ
      SZZW=SZZW*EEJJ
      TXYW=TXYW*EEJJ
C
  300 IF(II.EQ.1) ALPA1=ALPO
      IF(II.NE.1) ALPA1=ALPA
CCC   IF(ALPA1.LE.ALPP) ALPA1=ALPP
      EJP=EJ1
      RETURN
      END
C
C
      SUBROUTINE PLAST(P1,Y1,JO,AM,C,OK,PBP,P,EJ,EJO,EJJ)
C
C
      IMPLICIT REAL*8(A-H,O-Z)
C
      PK=OK+C*P1
      PP=.5*(P1+PK)
      PM=.5*(P1-PK)
C
C---PBP,EJ ARE PREVIOUS POINT FOT STARTING POINTS
C
      II=1
      PU1=PBP
      EJ1=EJ
C
C---JACOBIAN
C
   10 AJ11=2.*(PU1-PM)/PP/PP
      AJ12=2.*EJ1/Y1/Y1
      AJ21=4.*(EJ1/Y1/Y1-(EJ1-EJO)/PP/PP)
      AJ22=4.*((PU1-P)/Y1/Y1-(PU1-PM)/PP/PP)
      DET=AJ11*AJ22-AJ12*AJ21
C
      GG=(PU1-PM)*(PU1-PM)/PP/PP+EJ1*EJ1/Y1/Y1-1.
      FF=4.*(EJ1*(PU1-P)/Y1/Y1-(PU1-PM)*(EJ1-EJO)/PP/PP)
C
      PU2=-(AJ22*GG-AJ12*FF)/DET+PU1
      EJ2=EJ1-(AJ11*FF-AJ21*GG)/DET
C
      EBB=1.D+02
      STOC=DABS(PU2-PU1)
      STOD=DABS(EJ2-EJ1)
```

```
      IF(STOC.LE.ERR.AND.STOD.LE.ERR) GO TO 20
      WRITE(3,1000) PU2,EJJ,GG,FF,P1,Y1,PK,PP,PM,PR2,P,EC,EJO
 1000 FORMAT(13E10.5)

      P1=PU2
      EJJ=EJJ
      II=II+1
      IF(II.GE.50) WRITE(3,1111)
 1111 FORMAT(1X,'NEWTON METHOD FOR PLASTIC CONVERGE NOT')

      IF(II.GE.50) CALL EXIT
      IF(II.LT.50) GO TO 10
   20 P=PU2
      EJJ=EJJ

      WRITE
      END
```


(The reverse of this page is blank.)